THE UNIVERSITY OF ADELAIDE
AUSTRALIA

SUB CRUCE LUMEN

Application of Fractional Flow Theory to Foams in Porous Media

Submitted by: Zulfiqar Firoze Dholkawala

Submitted for: The degree of Master of Engineering Science in Petroleum

Submitted on: 7th February 2006

Submitted to: Australian School of Petroleum,
University of Adelaide.

Table of contents

Abstract

Due to its low viscosity and density, gas phase injected into porous media leads to viscous fingering, gravity segregation and channelling. The ability of foam to reduce gas mobility helps mitigate these problems by improving the sweep profile and increasing overall oil recovery. Although foam is believed to be a promising means to improve oil recovery, accurate prediction of its performance is hampered due to complicated foam rheology in porous media.

Mechanisms of foam displacement in porous media are investigated by the fractional flow theory in this study, incorporating fully mechanistic foam descriptions. During the change in total injection velocity by 8.15 times, the shape of fractional flow curves changes significantly, which in turn affects sweep efficiency and pressure profile markedly. The analytical solutions are in good agreement with recent mechanistic foam simulations in terms of foam texture, location of displacement front, saturation profile and pressure distribution.

The fractional flow theory with a new foam model in this study explains many features of conventional foam-generation experiments successfully: a weak-foam state at low injection velocity and a strong-foam state at high injection velocity, the transition from weak-foam to strong-foam state with a stepwise increase in injection velocity, the hysteresis associated with foam generation, and the effect of foam quality on foam generation. It should also be noted that the catastrophic nature of foam rheology observed in recent experimental and modelling studies are fully captured showing multiple solutions corresponding to weak-, intermediate- and strong-foam states. Construction of a three-dimensional surface of fractional flow curves makes it possible to analyze complicated foam mechanisms more conveniently.

When applied to gas injection (*i.e.*, fractional flow of water = 0), the method in this study shows that there exist two possible solutions: one with an immediate attainment of strong-foam state, exhibiting the water saturation behind the shock front near the limiting water saturation; and the other a weak-foam state with a long tail of spreading waves. Foam simulation shows that the selection between the two solutions is determined by the value of a

dynamic parameter, which describes how actively lamellae are created and destroyed in porous media.

Statement of Originality

- This thesis is an original effort and contains no material which has been accepted for the award of any other degree or diploma in any university or other tertiary institution and that, to the best of my knowledge and belief, the thesis contains no material previously published or written by another person, except where due reference is made in the text of the thesis.

- I give consent to this copy of my thesis, when deposited in the University Library, being made available in all forms of media, now or hereafter known.

Zulfiqar F. Dholkawala

12/06/2006

Acknowledgements

This thesis is dedicated to the memory of my late father Firoze Yahya Dholkawala. The submission of this thesis brings me a step closer to fulfilling his vision of seeing me successful in life.

My deepest gratitude to my principal supervisor Dr. Seung Ihl Kam who from day one has given me all the time, patience and support, and has shared with me his technical knowledge on this subject, without which the completion of this research would have been impossible. To my co-supervisor, Prof. Hemanta Sarma, a big thankyou for his moral support and invaluable non-academic advice.

Thanks too, to Santos Ltd. for providing me with the "Santos Scholarship" to pursue this Master's degree.

I also appreciate the help extended by the administration and technical staff of the Australian School of Petroleum, especially Yvonne, Janet and Eileen for taking care of those potential glitches and little formalities that I never knew even existed.

I am grateful to my colleague Thivanka for rendering his troubleshooting skills whenever required and to my friend Nicole for proof-reading this manuscript. And of course, not to forget all my fellow researchers on the '3rd floor-Room No. 302' with whom I have spent some wonderful days devising innovative excuses not to work.

Finally and most importantly I would like to thank all members of my 'family forest'. Special credit towards the completion of this thesis goes to my grandmother Shireen Fanaswala for constantly pestering God to look after me, to my mother Mohsina Dholkawala and my sister Shakera Khan for their unconditional love and understanding, numerous sacrifices and steadfast belief in my abilities, and to my aunt Munira Cementwala for her relentless encouragement.

List of Figures

Nomenclature

C_c	=	model parameter
C_f	=	model parameter
C_g	=	model parameter
f_g	=	gas fractional flow (gas injected volume fraction), usually expressed as %
f_g^*	=	value of f_g that divides strong foam into low-quality and high-quality regimes
f_w	=	water fractional flow (injected liquid volume fraction), usually expressed as a fraction < 1
h	=	film thickness
h^*	=	critical film thickness
k	=	permeability, units m^2 in calculations but reported in text as Darcy
k_{rg}^o	=	gas relative permeability in absence of foam
k_{rg}^f	=	gas relative permeability in presence of foam
k_{rw}	=	water relative permeability
m	=	model parameter
n	=	model parameter
n_f	=	foam texture or density (inversely related to bubble size); lamellae/unit volume of gas (m^{-3})
n_f^{max}	=	foam texture in the low-quality regime; maximum attainable value of n_f
N	=	total number of grid blocks in finite-difference simulation
P_c	=	capillary pressure (Pa)
P_c^*	=	limiting capillary pressure (Pa)
P_c^e	=	capillary entry pressure (Pa)
P_c^{sn}	=	capillary pressure for snap-off (Pa)
Δp	=	pressure drop (Pa)
∇p	=	magnitude of pressure gradient (Pa/m)
∇p^{min}	=	minimum pressure gradient for lamella mobilization (Pa/m)
r_c	=	rate of lamella destruction per unit volume of gas phase
r_g	=	rate of lamella creation per unit volume of gas phase
S_{gr}	=	residual gas saturation
S_w	=	water saturation
S_{wc}	=	connate water saturation

S_{wI} = water saturation at initial condition

S_{wJ} = water saturation at injection condition

S_w^* = water saturation at limiting capillary pressure P_c^*

u_g = gas volumetric flux or superficial velocity (m/s)

u_t = total volumetric flux or superficial velocity (m/s), i.e. (u_g+u_w)

u_w = water volumetric flux or superficial velocity (m/s)

Δx = grid-block size in finite-difference simulation

Greek Symbols

ϕ = porosity

μ_g^f = effective gas viscosity in presence of foam (Pa·s)

μ_g^o = gas viscosity in absence of foam (Pa·s)

μ_w = water viscosity

σ = gas-liquid interfacial tension

Subscripts and Superscripts

I = initial condition of core

J = property of injected fluids

w = water

g = gas

Dimensionless numbers

N_c = dimensionless capillary number in Ransohoff and Radke [1988]

N_{cL} = dimensionless capillary number in Tanzil [2001]

Publications

Refereed journal publication

- Dholkawala, Z.F., Sarma, H.K. and Kam, S.I., 2005. "**Application of Fractional Flow Theory to Foams in Porous Media**", accepted for publication in the Journal of Petroleum Science and Engineering, September.

Refereed conference paper

- Dholkawala, Z.F. and Kam, S.I., 2005. "**Modelling of Foam Rheology in Porous Media**", presented at the 5th IWA International Symposium on Wastewater Reclamation and Reuse for Sustainability, Jeju, Korea, November 8-11.

1. Introduction

Foam, an agglomeration of bubbles, is a colloidal dispersion in which a gas is dispersed in a continuous surfactant-laden liquid phase [Bikerman, 1973; Schramm, 1994]. Once contained within tiny pores, its characteristics strongly depend on the stability of thin liquid films called "lamellae" [Kovscek and Radke, 1994; Rossen, 1996]. Foams in porous media are used in near-wellbore flow treatments such as foam-acid matrix stimulation and blocking of unwanted phases [Cheng *et al.*, 2002; Kam *et al.*, 2003; Wassmuth *et al.*, 2004], in shallow subsurface environmental remediation [Hirasaki *et al.*, 1997; Hirasaki *et al.*, 2000; Mamun *et al.*, 2002] and in field-scale enhanced oil recovery (EOR) processes [Hirasaki *et al.*, 1989; Patzek and Koinis, 1990; Hanssen *et al.*, 1994; Wang *et al.*, 2001; Blaker *et al.*, 2002] in order to control the mobility of gas phase and overcome in-situ permeability variations.

Foam can be applied by simultaneously injecting gas and surfactant solution or alternating gas with surfactant solution. Foam quality (f_g), defined as the fraction of gas phase in the mixture (*i.e.*, the volumetric flux of gas to the total volumetric flux of gas and liquid), is an important design parameter in field applications. In spite of decades of foam research, much of foam behaviour in porous media still remains unresolved and requires understanding of complex foam rheology.

The fractional flow theory describes the physics of miscible and immiscible displacements in porous media, in which the governing hyperbolic partial differential equations are solved analytically by a mathematical technique called the method of characteristics. The fractional flow curves constructed theoretically by plotting water fractional flow (f_w) in y-axis and water saturation (S_w) in x-axis, were first presented and solved by Buckley and Leverett [1941]. Since then, a number of studies have further developed the theory to account for a wide range of applications in secondary and tertiary oil recovery [Dake, 1978; Pope, 1980; Rossen *et al.*, 1995; Zeilinger, 1996]. Fractional flow solutions for foam applications have been presented by Rossen and Zhou [1995] in which a mobility reduction factor is, for simplicity, assumed to represent foam mechanisms. Although the fractional flow theory requires simplifying assumptions such as one-dimensional displacement, Newtonian viscosity, no viscous fingering, no capillary-pressure gradients, no physical dispersion, incompressible phases and immediate attainment of local steady

state, many of the assumptions can be relaxed to some extent and therefore the solutions are still able to capture complex displacement mechanisms. Details on the validity of fractional flow solutions are available elsewhere [Dake, 1978; Lake, 1989; Rossen *et al.*, 1999]. Different types of gas phases have been applied in many different laboratory and field studies including hydrocarbon gases, air, nitrogen (N_2) and carbon dioxide (CO_2).

This study, for the first time, presents how to apply fractional flow method to the case of foams in a wide range of injection velocities, reproducing the trends of recent experimental studies, including foam catastrophe and three different foam states (weak-, intermediate-, and strong-foam state) [Gauglitz *et al.*, 2002; Kam and Rossen, 2003]. Complex foam behaviour in porous media predicted by the fractional flow solutions introduced in this study is validated by the recently developed foam-simulation technique [Kam *et al.*, 2004]. A mathematical model incorporating mechanistic equations of foam physics in porous media fully accounts for the nonlinear relationship between the injection rate and pressure gradient, resulting from the interplay between the rates of lamella creation and coalescence.

This study is a necessary step towards reliable predictions for foam applications in constant-pressure or constant-rate gas injection, surfactant-alternating-gas (SAG) process, and foam injection at very dry conditions.

2. Literature Review

The rheological properties of foam in porous media are complicated in that the number of lamellae present governs the flow characteristics, including viscosity, relative permeability, yield stress, fluid distribution, and interactions between fluids. "Foam texture", defined as the number of lamellae per unit volume, is used to quantify the bubble population. Although foam texture is of prime importance in foam rheology, there are currently no reliable experimental techniques to measure it directly. Rather, it is a common practice to infer foam texture indirectly from the pressure profile or apparent gas viscosity data. This chapter provides a summary of key concepts and recent developments in foam research followed by the objectives of this study.

2.1. Weak foam vs. strong foam

Experiments at steady gas and liquid injection show that there are two foam states in porous media: coarsely textured foam (or a small number of lamellae with a large bubble size) is referred to as "weak foam" because it provides a moderate reduction in gas mobility; whereas finely textured foam (or a large number of lamellae with a small bubble size) is referred to as "strong foam" because it reduces gas mobility remarkably. Fig. 2-1 schematically compares conventional gas-water flow, weak foam, and strong foam. The presence of lamellae tends to divert the flow of wetting phase to smaller pores. As a result, water saturation (S_w) is markedly lower with strong foam than with conventional gas-liquid flow. It should be noted that a region called “Plateau border”, in which the majority of water accumulates, is formed once a lamella touches a solid surface as shown in Fig. 2-1.

2.2. Mechanisms of lamella coalescence and creation

For accurate prediction of foam behaviour in porous media, one needs to keep track of mechanisms of lamella creation and coalescence in a mechanistic manner. These pore-level events are described in the following sections.

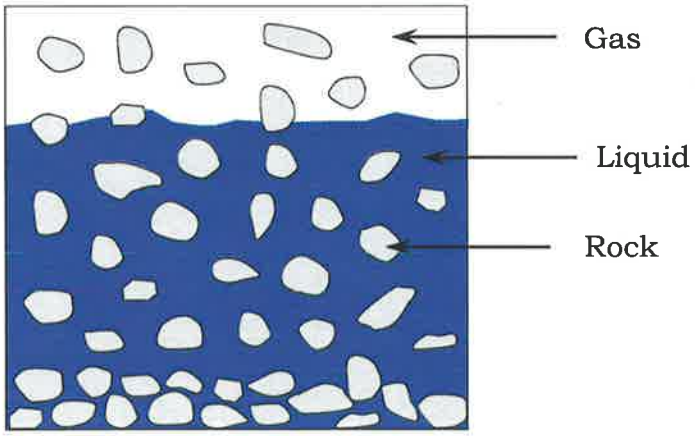

No Foam

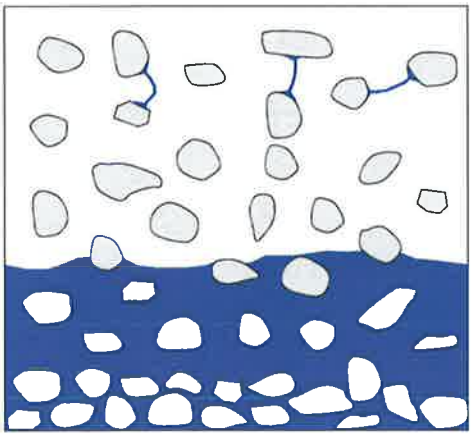

Weak Foam

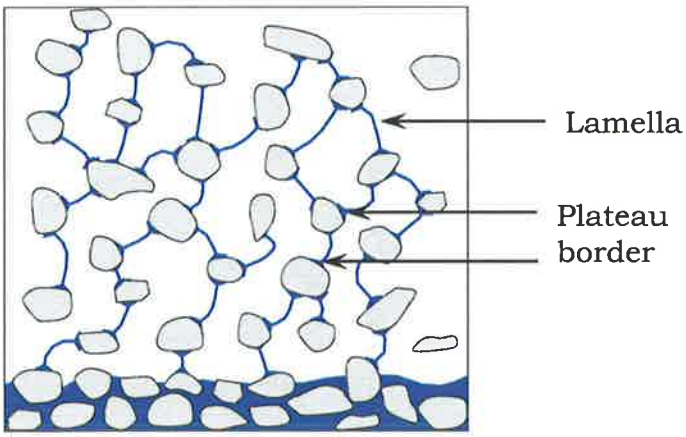

Strong Foam

Fig. 2-1. Comparison between conventional gas-liquid two-phase flow and foams (weak and strong) in porous media.

2.2.1. Lamella coalescence

Lamellae can be destroyed by many different factors such as capillary force, gas diffusion, liquid evaporation/condensation, presence of destabilizing phases and mechanical disturbance [Bikerman, 1973; Chambers and Radke, 1991; Nguyen *et al.*, 2000]. The first two have major impacts on foam in porous media as further explained below.

2.2.1.1. Capillary pressure

Capillary suction coalescence is widely believed to be the principal mechanism of foam destruction [Derjaguin and Obukhov, 1936; Khatib *et al.*, 1988; Jiménez and Radke, 1989; Chambers and Radke, 1991]. Lamella coalescence is a consequence of film instability predicted by thermodynamics, implying that a system moves towards minimizing its free energy by reducing interfacial area between different phases [Bikerman, 1973]. Higher capillary pressure (P_c) induces water to be imbibed from the film to the Plateau border, eventually causing the film to rupture. Once surfactant molecules are present at the gas-liquid interface, disjoining pressure slows down film drainage and thus foam can survive for a relatively long time [Khatib *et al.*, 1988; Aronson *et al.*, 1994; Rossen and Zhou, 1995].

The relation between disjoining pressure and film thickness is shown in Fig. 2-2. A film cannot sustain if its thickness (h) goes below the critical thickness, h^*. When the film is relatively thick ($h > h^*$), the repulsive forces between surfactant molecules is dominant, providing film stability. As the film becomes thinner (h approaching h^*), disjoining pressure increases monotonically until the thickness reaches the critical thickness (h^*) at which disjoining pressure is at its maximum (P_c^*). The film collapses when h becomes less than h^*.

Khatib *et al.* [1988], among many, show that foam stability within porous media is strongly affected by capillary pressure (P_c) based on multiphase flow experiments in beadpacks, finding an abrupt transition from strong foam to weak foam near a specific value of capillary pressure above which lamella cannot sustain. This value of P_c is called the limiting capillary pressure or P_c^*. Since capillary pressure is related to water saturation in porous media, there is a water saturation that corresponds to P_c^*, called limiting water saturation (S_w^*).

Fig. 2-3 shows a schematic of a lamella in motion along complicated pore geometry. The lamella stretches at pore bodies and squeezes at pore throats repeatedly as it travels. The thickness of the film also becomes thin and thick accordingly. The amount of surrounding liquid and the rate of liquid transport between the film and Plateau border are vital to lamella stability [Jiménez and Radke, 1989]. This implies that a lamella in dynamic motion tends to be less stable than that in a static condition.

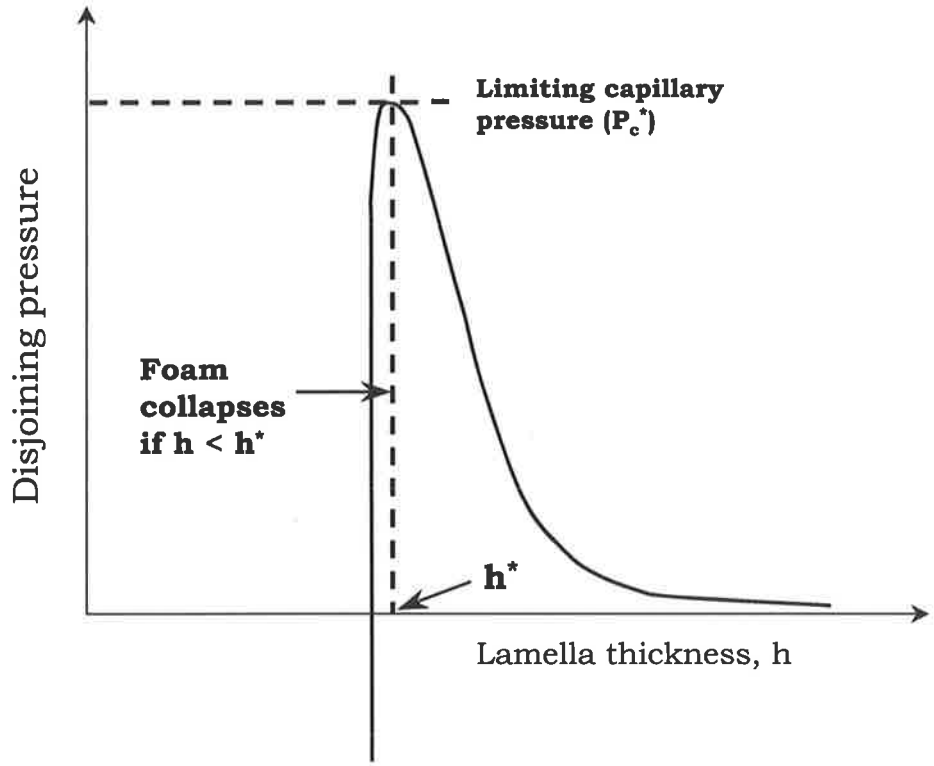

Fig. 2-2. Schematic of disjoining pressure as a function of lamella thickness (following Derjaguin and Obukhov, 1936).

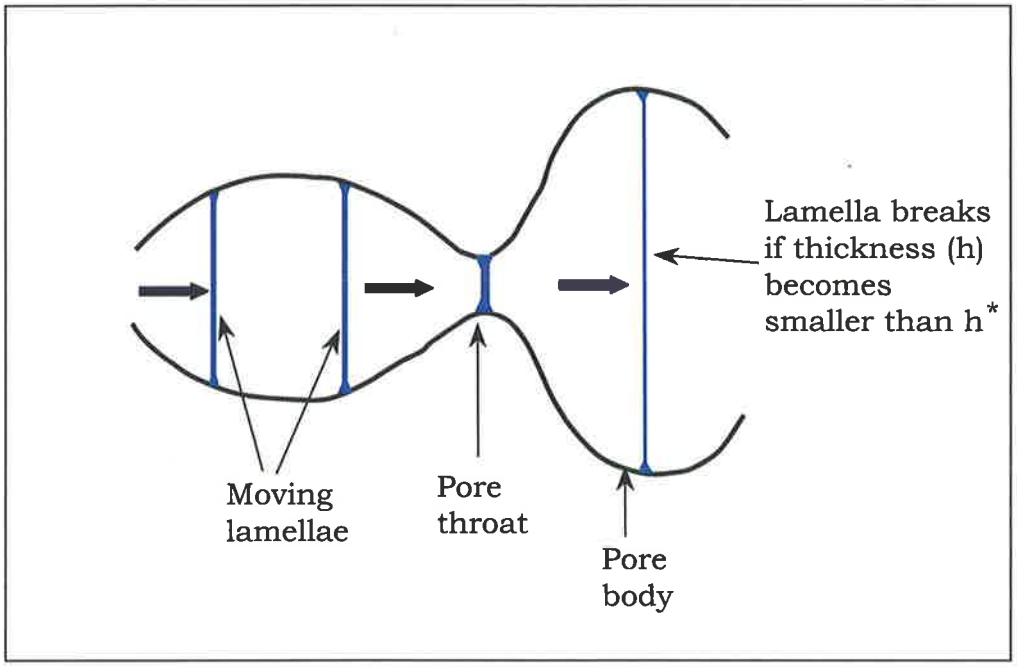

Fig. 2-3. Schematic of a moving lamella approaching coalescence in a typical pore structure (following Jiménez and Radke, 1989).

2.2.1.2. Gas diffusion

Fig. 2-4 shows the role of diffusion on foam texture. When bubbles of different sizes are placed close to one another in bulk foam [*cf.,* Fig. 2-4(a)], the mass of gas in smaller bubbles is transported into larger bubbles by diffusion. The rate of this transport is governed primarily by the curvature of the bubbles (or, capillary pressure). As diffusion takes place, smaller bubbles shrink more rapidly and finally gas and liquid phases become segregated [Bikerman, 1973; Chambers and Radke, 1991]. When trapped in porous media, bubbles merge by diffusion as in the case of bulk foam. Due to geometric constraints, however, diffusion comes to an end when individual bubbles become roughly as big as pore size and thus the interface has zero curvature [*cf.,* Fig. 2-4(b)]. For modelling purposes, one can use the concept of minimum bubble size (or maximum foam texture (n_f^{max}) equivalently) to account for this effect.

2.2.2. Lamella creation

Many studies have identified three principal mechanisms of in-situ lamella creation [Ransohoff and Radke, 1988; Rossen, 1996; Hirasaki *et al.*, 1997]: lamellae can be left behind during a drainage process ("leave behind" mechanism); a non-wetting gas phase can be snapped off when P_c fluctuates sufficiently ("snap-off" mechanism); and a pre-existing lamella can first be mobilized by the pressure gradient (∇p) and subsequently divided into many at the pore junctions downstream ("lamella mobilization and division" mechanism). Recent studies suggest that "lamella mobilization and division" should be the main lamella-creation mechanism during steady gas-liquid flow [Gauglitz *et al.*, 2002; Kam and Rossen, 2003; Tanzil, 2001]. More detailed reviews on these mechanisms are explained below.

2.2.2.1. Leave-behind

Upon the invasion of non-wetting gas phase, lamellae can be left behind as the fingers of gas phase grow downstream. The lamellae remain stable as long as the capillary pressure of the system kept is low (*i.e.,* sufficient wetting phase liquid is present). Fig. 2-5 shows lamellae created by leave-behind, usually thick and oriented parallel to the direction of flow. The gas phase is continuous, resulting in weak foam with a modest reduction in gas mobility.

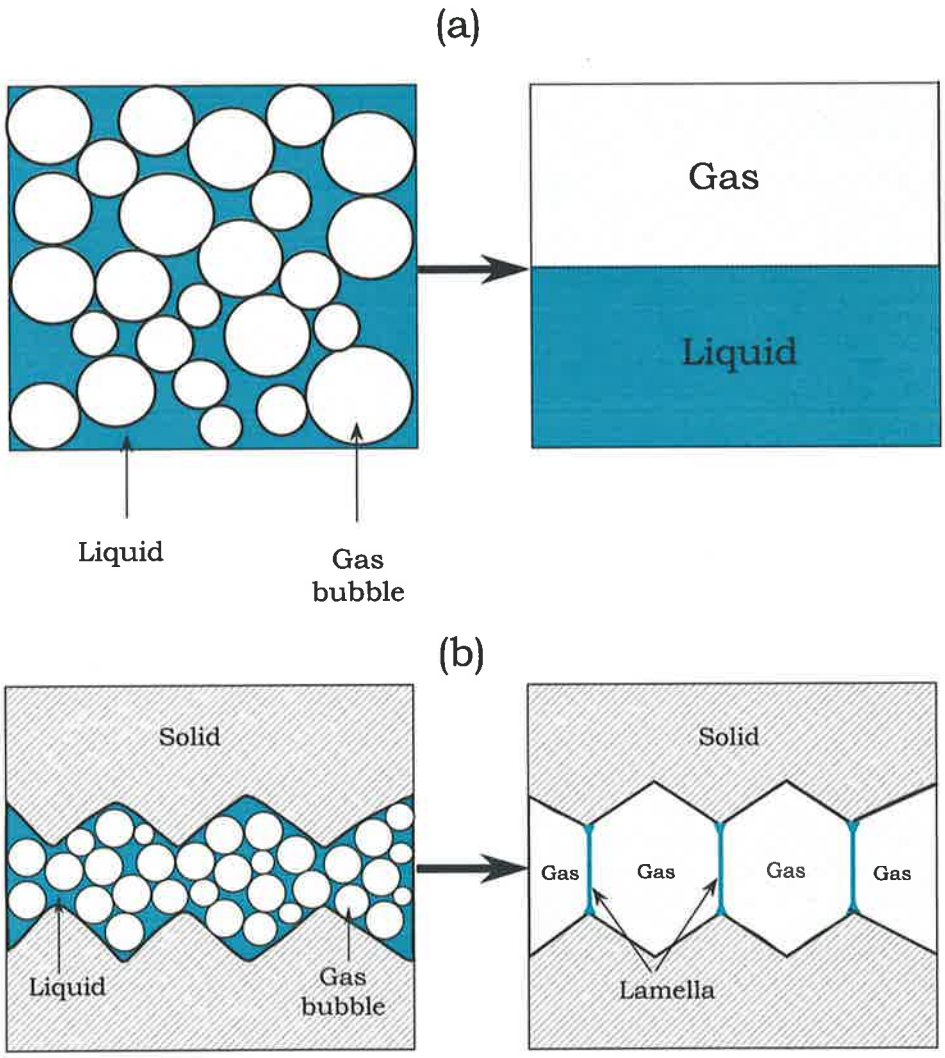

Fig. 2-4. Schematic of bubbles merging as a result of diffusion: (a) diffusion in bulk foam and (b) diffusion in porous media.

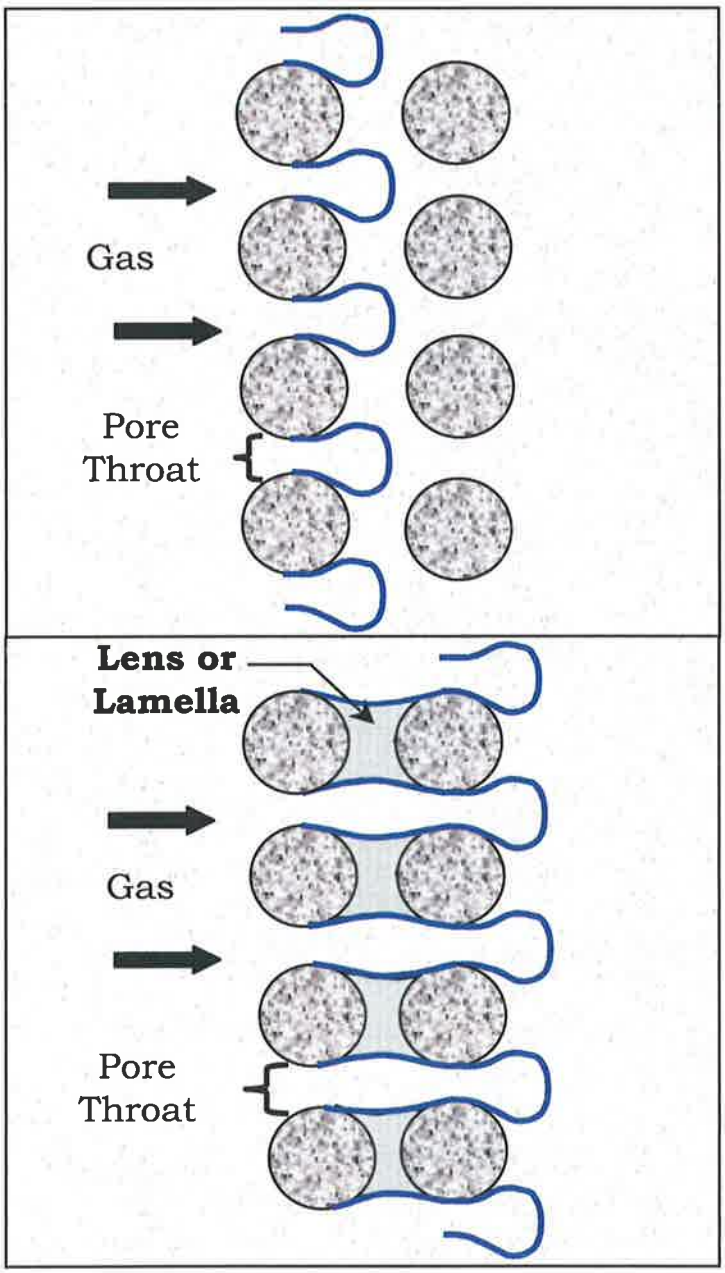

Fig. 2-5. Lamellae created by "leave-behind" mechanism during drainage process.

2.2.2.2. Snap-off

Snap-off is a mechanism that may create a large number of lamella effectively [Kovscek and Radke, 1994]. Snap-off takes place when capillary pressure fluctuates significantly. Repetitive snap-off mechanism as shown in Fig. 2-6, sometimes called "Roof" snap-off, has been widely employed in foam modelling due to its simplicity [Falls *et al.*, 1988; Kovscek *et al.*, 1995; Bertin *et al.*, 1998]. In this mechanism, the capillary pressure (P_c) must be higher than the capillary entry pressure (P_c^e) for gas to invade a pore throat, but then fall below the capillary pressure for snap-off (P_c^{sn}). P_c^{sn} is known to be dependent on pore geometry. For example, for a pore structure with a circular cross-sectional area, P_c^{sn} is roughly equal to ½ P_c^e. Detailed discussion on snap-off mechanism can be found elsewhere [Schramm, 1994].

2.2.2.3. Lamella mobilization and division

Fig. 2-7 explains lamella mobilization and division mechanism. When a moving bubble encounters a point where flow branches in two directions, the bubble may break or divide into two separate bubbles. Because successful division can lead to a large number of lamellae rapidly, lamella mobilization and division is also believed to create strong foam that exhibits a drastic decrease in gas mobility.

2.2.3. Significance of lamella creation mechanism

Although many mechanistic foam models use the concept of Roof snap-off to describe in-situ lamella creation, Rossen [2000] argues that this mechanism is irrelevant to foam modelling in porous media and thus can be misleading because a singly constricted tube is not a true representation of pore shape in porous rocks. Rossen [2000] proposes the use of a doubly constricted tube with two pore throats instead, *i.e.*, a tube with finite downstream volume. His experiment shows that once the pore body is entirely occupied by bubbles and gas begins to move towards the downstream throat, the process of repeated snap-off ceases. Hence, snap-off cannot explain lamella creation in steady gas and liquid flow.

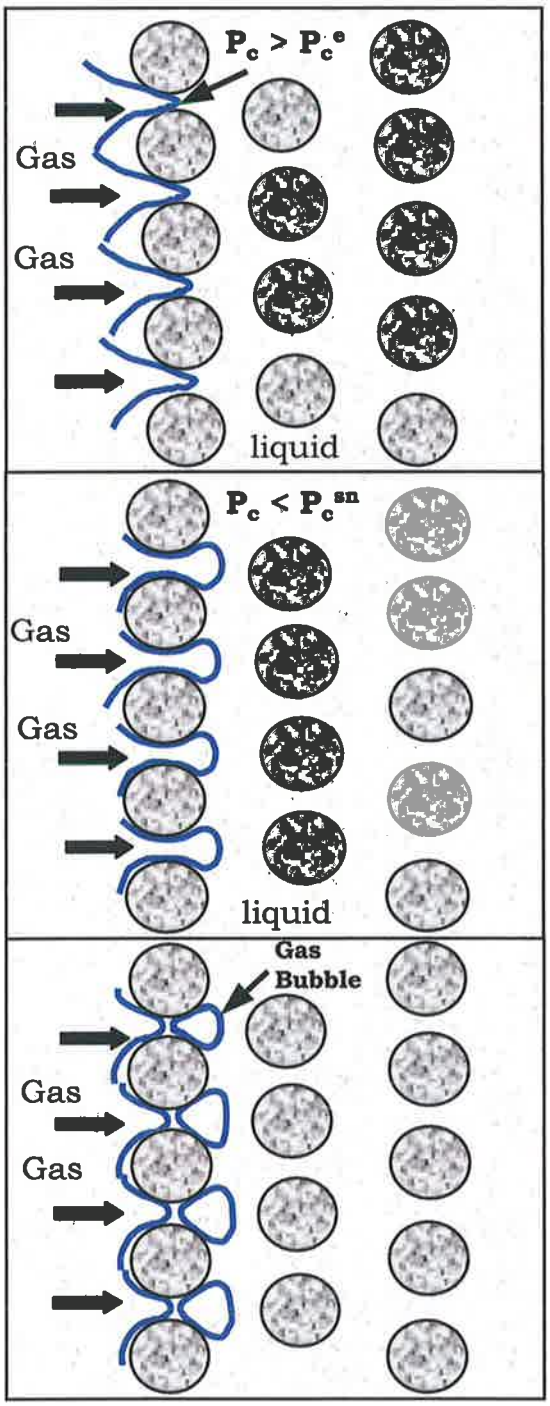

Fig. 2-6. Gas bubbles created by snap-off: P_c should be greater than capillary entry pressure (P_c^e) for gas to enter the throat and should then drop below the capillary pressure required for snap-off (P_c^{sn}).

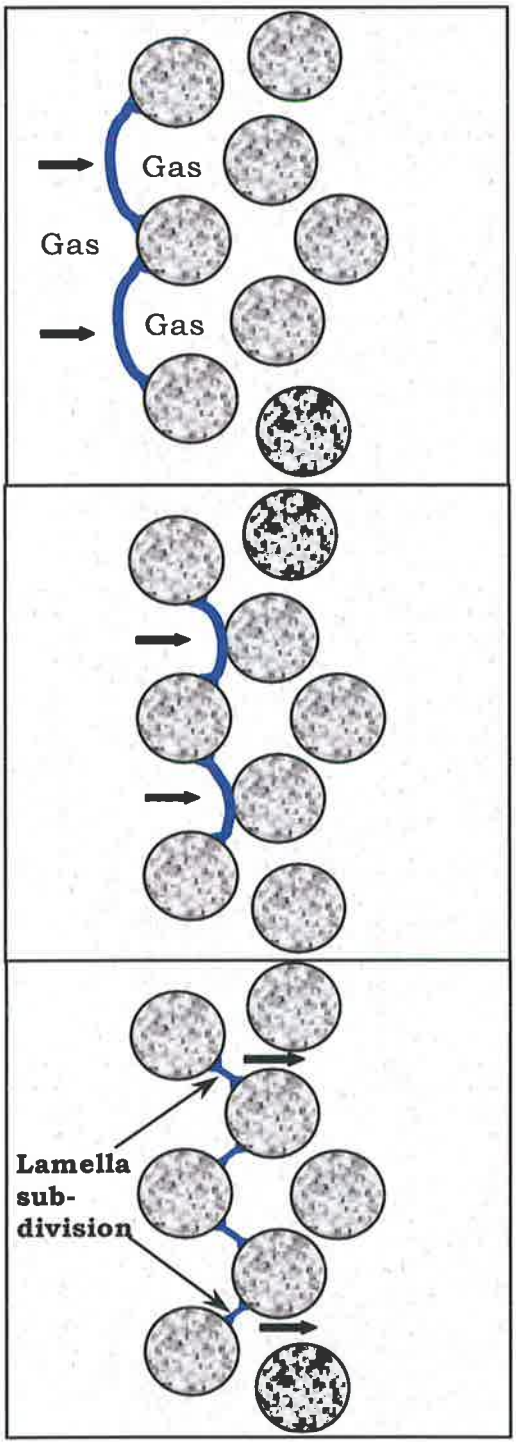

Fig. 2-7. Lamella creation by mobilization and division mechanism.

Alternately, many recent studies on foam in porous media consider lamella mobilization and division to be the main mechanism of lamella creation [Rossen and Gauglitz, 1990; Tanzil *et al.*, 2002; Gauglitz *et al.*, 2002; Kam and Rossen, 2003]. This study follows lamella mobilization and division as the main lamella-creation mechanism.

2.3. Foam generation in porous media

"Foam generation" is defined as the state at which the rate of lamella creation greatly exceeds the rate of lamella destruction [Falls *et al.*, 1988; Kovscek and Radke, 1994]. A number of experiments indicate the presence of a pressure gradient (∇p) or injection velocity above which weak foam is suddenly converted into strong foam [Ransohoff and Radke, 1988; Rossen and Gauglitz, 1990; Friedmann *et al.*, 1991; Tanzil, 2001]. This sudden change accompanied by a drastic reduction in gas mobility is referred to as foam generation.

Estimating the onset of foam generation has been a challenge in foam research. Falls *et al.* [1988] conducted experiments on both homogeneous and heterogeneous beadpacks. Their experiments show that a sudden increase in permeability in the flow direction causes liquid to accumulate and snap-off to occur. Ransohoff and Radke [1988] injected gas at constant, predetermined flow rates into an initially liquid saturated beadpack. Efforts were made to find a relationship between foam generation and a dimensionless capillary number (N_c) given by:

$$N_c = \frac{\mu_{nw} u L R_g}{\sigma k k_{rnw}} \qquad (2\text{-}1)$$

where μ_{nw} is the viscosity of the non-wetting (gas) phase, u is the total superficial velocity, L is the length of the experimental core, R_g is the grain radius in the core, σ is the gas-liquid surface tension, k is the absolute permeability, and k_{rnw} is the relative permeability of the gas phase. Their experiments show that when the capillary number goes above a critical capillary number (N_c^*), the relative permeability to the gas phase dramatically decreases. Following Roof snap-off, they proposed the existence of

"germination sites" at which lamellae can be repeatedly created, eventually leading to fine-textured strong foam or foam generation.

Friedmann *et al.* [1991] injected gas and brine into a core at low velocity. The brine was then replaced by surfactant solution at the same low rate with no significant increase in pressure drop. Injection velocities were then raised in steps at fixed foam quality. They reported a minimum velocity for strong foam generation. Baghdikian and Handy [1991] conducted experiments at fixed flow rates and noticed a threshold value of pressure drop (Δp) for foam generation. An interesting fact observed by Shi [1996] was that once foam generation occurs at fixed foam quality, it is possible to maintain strong-foam state even below the flowrate at which foam generation was initiated. This type of hysteresis also appears in Kibodeaux and Rossen [1997].

Chou [1991] investigated N_2 and CO_2 foam generation in Berea cores under various pressure gradients, surfactant formulations, foam qualities, flow rates and core lengths. No abrupt change in pressure gradient was observed even at the onset of foam generation. He also found that formation of strong foam depends on the initial saturation of the core, which is consistent with other foam experiments with N_2 [Friedmann and Jensen, 1986; Rossen and Gauglitz, 1990; Kovscek and Radke, 1994].

Rossen and Gauglitz [1990] proposed a model based on percolation theory for foam generation triggered by lamella mobilization and division. According to their theory, the number of lamellae awaiting mobilization within the porous medium depends on the capillary pressure which is affected by water fractional flow (f_w) and water saturation (S_w). Their study shows that there is a minimum pressure gradient (∇p^{min}) required to mobilize the lamellae during steady flow of gas and liquid.

Tanzil [2001] attempted to fit experiments using a capillary number (N_{cL}) given by:

$$N_{cL} = \frac{\Delta p_L}{\sigma}\sqrt{\frac{k}{\phi}} \qquad (2\text{-}2)$$

where Δp_L is the pressure drop measured over the system length, σ is the gas-liquid surface tension, k is the absolute permeability, and ϕ is the porosity. In

his study, foam generation occurred at a critical capillary number (N^*_{cL}). In contrast to Ransohoff and Radke [1988], however, Tanzil's [2001] capillary number was based on lamella mobilization and induced by pressure gradient. In the extension of this work, Tanzil *et al.* [2002] suggested the use of a critical normalized pressure gradient ($N^*_{\nabla p}$) for steady gas and liquid injection and a critical normalized pressure drop ($N^*_{\Delta p}$) for transient displacement.

2.4. Two steady-state strong foam regimes

Osterloh and Jante [1992] first found two remarkably different flow patterns once strong foams are achieved in sandpacks. Other studies also confirmed the same behaviour in a wide range of permeabilities, surfactant concentrations and formulations, different types of gas phase and temperatures [Alvarez *et al.*, 2001; Mamun *et al.*, 2002; Kam *et al.*, 2003]. Fig. 2-8 shows one example from Alvarez *et al.*'s [2001] study in which the steady-state ∇p was measured during co-injection of N_2 and surfactant solution. Fig. 2-8 clearly shows two different flow regimes: a high-quality regime (*i.e.,* upper-left portion of the figure) in which the steady-state pressure gradient is nearly independent of gas flow rate u_g and a low-quality regime (*i.e.,* lower-right portion of the figure) in which the pressure gradient is almost independent of liquid flow rate u_w. Accounting for the fact that any straight line drawn from the origin in Fig. 2-8 represents a fixed foam quality, there is a value of f_g, called "f_g^*", that divides this domain into two flow regimes. Previous studies found that the two regimes are governed by different mechanisms: the high-quality regime by bubble coalescence near the limiting capillary pressure (P_c^*) and the low-quality regime by bubble trapping and mobilization [Khatib *et al.*, 1988; Rossen and Wang, 1999; Alvarez *et al.*, 2001]. It is believed that bubble size in the low-quality regime is kept roughly the same as pore size and thus foam texture (n_f) is almost fixed at its maximum (n_f^{max}).

2.5. Previous modelling efforts

Most models on foam generation and propagation can be grouped under the following categories: percolation-based pore network models, empirical models, population balance models, and fractional flow models.

2.5.1. Pore network models

Percolation theory describes the behavior of connected clusters in a random domain. In relation to porous media, percolation theory concerns the movement and filtering of fluids through porous materials. Existing literature lists models such as capillary bundle, Bethe tree, cubic and square lattices as commonly used network topologies [Rossen and Gauglitz, 1990; Chou, 1990; Kharabaf and Yortsos, 1996; Chen *et al.*, 2004].

Chou [1990] developed a statistical network model containing pore throat and pore body size distribution functions representative of the pore geometry. The theory was based on the assumption that lamellae may break and re-form, and that lamellae are generated only in those pores in which the body to throat ratio is above some critical value for snap-off to occur.

Rossen and Gauglitz [1990] developed a percolation theory based model that indicates a minimum pressure gradient or injection rate required to generate foam. Rossen and Wang's model [1997] captures foam behaviour within the low-quality strong-foam regime in foam-assisted acid-diversion processes. While models for high-quality regime are based on the feedback mechanism near the limiting capillary pressure, this model assumes that bubble size is fixed and independent of liquid and gas flowrates in the low-quality strong-foam regime as indirectly evidenced by Alvarez *et al.* [2001].

Kharabaf and Yortsos's model [1996] is based on snap-off mechanism for initial bubble creation and determines a minimum pressure gradient required to mobilize the lamella. Snap-off probability and pore size distributions are also taken into consideration. They claimed that their pore network model for the first time simulates a dynamic invasion process.

Although network models can replicate pore-level behaviour, the computational time required is quite large. In addition, the results obtained are restricted due to the simplifying assumptions. The ability of network models to simulate transient displacement foam behaviour, which depends on a number of factors such as liquid saturation, foam quality and surfactant concentration, is debatable.

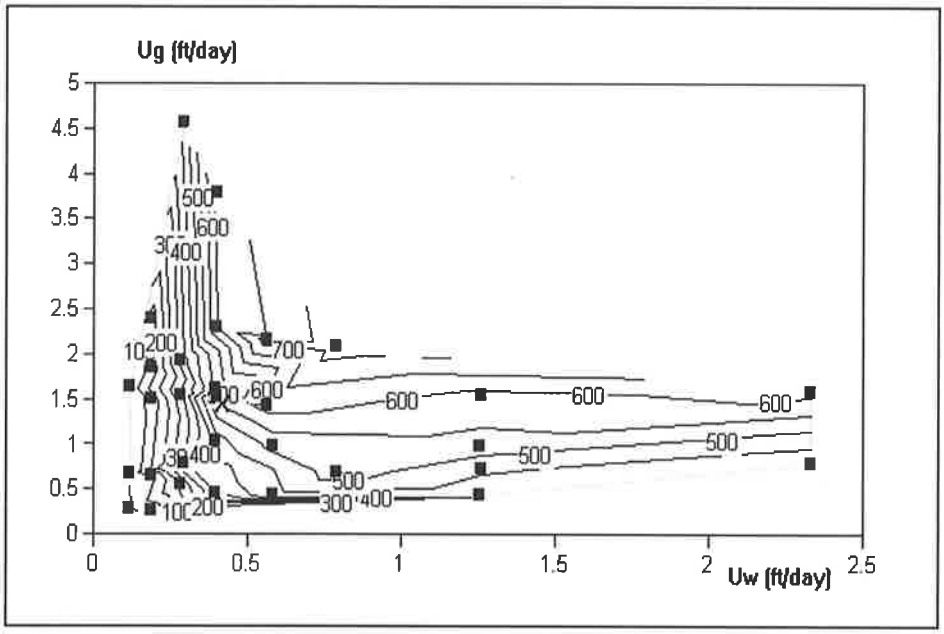

Fig. 2-8. Steady-state pressure gradient of strong foam as a function of gas (u_g) and liquid (u_w) volumetric fluxes in Alvarez *et al.* [2001]: vertical contours in the upper-left portion represents high-quality strong-foam regime (∇p independent of u_g) and horizontal contours in the lower-right portion represents low-quality strong-foam regime (∇p independent of u_w).

2.5.2. Empirical models

In empirical modelling, steady-state foam mobility, usually measured from core flood experiments, is accounted for within a range of surfactant concentrations, flow rates and permeabilities by using a number of mathematical correlations. Such correlations are incorporated into gas viscosity or gas relative permeability.

Mahmood *et al.* [1986] formulated a semi-analytical model to predict the recovery and pressure response during the flow of gas and surfactant solution. To accommodate change in flow behaviour in the presence of foam, they used an average value of gas mobility based on experimental observations. Marfoe and Kazemi [1987] developed a one-dimensional simulator for two-phase flow based on continuity equations. The modification for foam flow was made by increasing gas viscosity. The expression for gas viscosity included the effect of surfactant concentration, interstitial gas velocity, and water available for foaming. Fisher *et al.* [1990] developed two- and three-phase foam mobility models based on Khatib *et al.* [1988], explaning foam behaviour near the limiting capillary pressure. They expressed foam mobility in terms of critical relative mobilities, functions of gas velocity and surfactant concentration, and fractional flow of water. Experimental results for two-phase corefloods were in good agreement with modelling results.

An alternative method to describe flow behaviour in the presence of foam is the concept of "resistance factor" as defined by Chou [1991]. Resistance factor is defined as the ratio of the pressure drops, one with foam present and the other with no foam (*i.e.,* conventional gas and liquid flow), at the same injection rate and foam quality. Chang and Grigg [1996] calculated gas mobility in the presence of foam based on resistance factor data at a given surfactant formulation. Their model was built to accommodate a moderate amount of oil saturation.

The major drawback of empirical models is that they are not generic in nature. As a result, the dynamics of foam displacement in porous media cannot be implemented comprehensively. This is explained in further detail in the next section.

2.5.3. Population balance models

The population balance model is the most comprehensive tool to depict dynamic foam mechanisms. It tracks changes in foam mobility through a series of mathematical equations to update foam texture as a function of dynamics of in-situ lamella creation and coalescence. The conditions at the inlet and outlet are specified as boundary conditions and the initial saturation in the core is reflected as an initial condition for a series of partial differential equations. Compared to conventional two-phase simulations, foam simulation is more complex because of the interplay between lamella creation and destruction, foam viscosity, foam texture, trapped gas saturation, and gas yield stress, which should be updated at each time step. Most researchers believe foam texture to be the most crucial parameter in mechanistic foam simulation.

Different versions of the population balance model are available in literature. Falls *et al.* [1988] proposed a population balance for lamella creation based on a critical capillary pressure for snap-off. Results show that the occurrence of liquid accumulation causes snap-off when the permeability increases in the flow direction. Lamella destruction is unaccounted for in Falls *et al.* [1988]. Chang *et al.* [1990] include snap-off, lamella mobilization and leave-behind in their model. Snap-off or mobilization and division occurs above a critical gas velocity only. The lamella-destruction rate is based on the limiting capillary pressure. Friedmann *et al.* [1991] set the rate of lamella creation at zero below the critical velocity and, once the critical velocity was achieved, the rate was independent of velocity. The rate of lamella coalescence is proportional to the number of bubbles and also affected by surfactant formulation. Their model predictions for gas saturation and pressure drop agree well with experimental data. Based on the experimental work of Kovscek and Radke [1994], Kovscek *et al.'s* [1995] study with snap-off mechanism derives an expression for the net rate of foam generation as a function of liquid and gas interstitial velocities. The velocities in turn are dependent on the local liquid and gas saturations and the local pressure gradient. Similar to Chang *et al.* [1990], foam destruction is driven by the concept of limiting capillary pressure.

Although the population balance model provides the framework for foam modeling and simulation, different foam mechanisms are available in literature. This aspect is explained in detail later in this chapter.

2.5.4. Fractional flow models

The fractional-flow theory is used to describe the movement of miscible and immiscible fluids in a reservoir. Mathematical solutions to the fractional flow curves, termed the method of characteristics, were first provided by Buckley and Leverett [1941]. Since then, many studies have applied this concept to a wide range of applications [Pope, 1980; Lake, 1989; Rossen *et al.*, 1995; Zeilinger, 1996]. Recently, Zhou and Rossen [1995] have extended this theory to foam displacements with some simplifying assumptions. These include one-dimensional displacement; Newtonian mobilities; absence of viscous fingering, capillary-pressure gradients and physical dispersion; incompressible phases and immediate attainment of local steady state.

In the fractional flow theory, a wave diagram can be constructed from the fractional flow curve (*i.e.,* f_w vs. S_w), along with the initial and injection conditions to describe the displacement process. The results can be visualized in terms of saturation profile, effluent history, and time-distance diagram to keep track of shock and spreading waves. The slope at any saturation on the fractional flow curve represents the dimensionless velocity of the wave at that particular saturation. Initially, the saturation waves move with velocities equal to the slope (df_w/dS_w) on the curve at a particular value of S_w. However, discontinuities in saturation, called shock fronts, occur when the rearward waves of higher velocities overtake the forward waves of lower velocities [Lake, 1989]. Graphically, a shock occurs when the slope (df_w/dS_w) of the fractional flow curve does not increase monotonically from the injection condition 'J' to the initial condition 'I'.

2.6. Recent developments in foam research

Historically, the majority of the coreflood experiments for foams in porous media have been conducted by changing total injection rate at fixed foam quality. Gauglitz *et al.* [2002] performed two other types of experiments to study foam generation in porous media: at "*fixed* ∇p and fixed f_g", and at "*fixed* ∇p and fixed u_w". Their results, summarized by a three-dimensional (3D) surface of ∇p in z-axis and u_w and u_g in x and y- axes respectively as shown in Fig. 2-9, clearly indicates three distinct foam states: a weak-foam state at low ∇p (*i.e.,* the lower surface of Fig. 2-8), a strong-foam state at high ∇p (*i.e.,* the

upper surface of Fig. 2-8) and an unstable intermediate foam state in between. The 3D surface implies that foam rheology in porous media, similar to catastrophe theory [Poston and Stewart, 1978], is a multi-valued problem when u_w and u_g are fixed but a single-valued problem when ∇p is fixed. Discovery of the intermediate state at fixed ∇p also explains the hysteresis observed in a number of foam-generation studies [Shi, 1996; Kibodeaux and Rossen, 1997].

As an extension of Gauglitz *et al.*'s [2002] work, Kam and Rossen [2003] developed a new mathematical model based on "lamella mobilization and division". Although their work borrows from previous population balance models, it uses a lamella-creation mechanism that is a simple function of ∇p. As shown in Fig. 2-10, Kam and Rossen [2003] are able to predict the three foam states observed in Gauglitz *et al.*'s [2002] study. Furthermore, the model also reproduces the two steady-state strong-foam regimes: the high-quality regime (in which ∇p is independent of gas flow rate) and the low-quality regime (in which ∇p is independent of liquid flow rate).

Kam *et al.* [2004] incorporated Kam and Rossen's model [2003] into the framework of conventional gas-liquid two-phase simulation. Their study shows that foam simulation with ∇p-induced lamella creation mechanism successfully fits typical coreflood experiments. It also proves that the intermediate foam state, conjectured to be obtainable only in ∇p-fixed experiments, is intrinsically unstable in fixed rate experiments. Simulation results show good agreement with foam catastrophe suggested by Gauglitz *et al.* [2002].

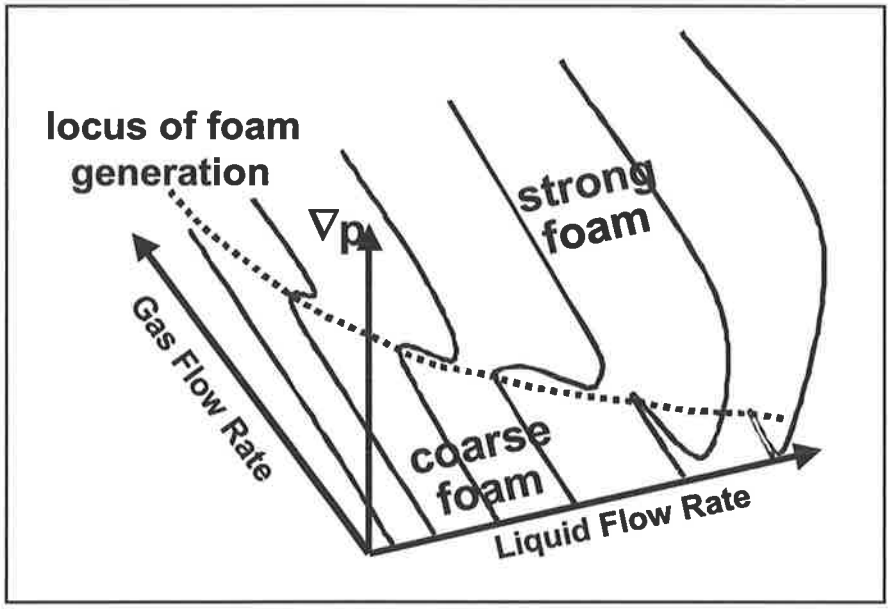

Fig. 2-9. Three-dimensional foam generation surface conjectured by Gauglitz *et al.* [2002]: the surface folds back and forth from weak-foam state to intermediate state, and eventually to strong-foam state at high pressure gradient.

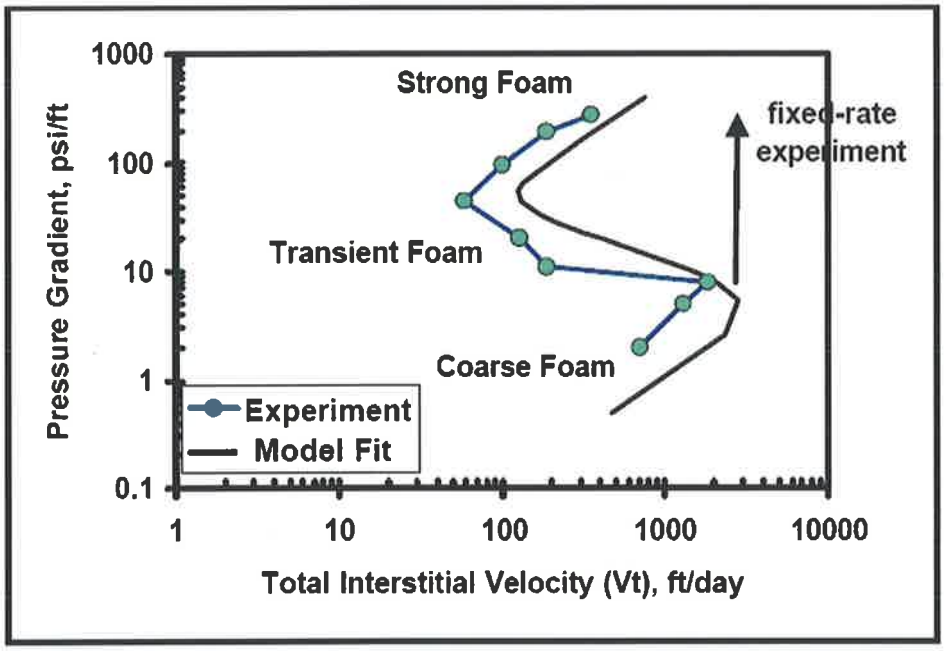

Fig. 2-10. Kam and Rossen's model [2003] fit to Gauglitz *et al.'s* [2002] experimental data at fixed ∇p and foam quality.

2.7. Objectives of this study

It should be emphasized that the model in Kam and Rossen [2003] and Kam *et al.* [2004] is the only population balance model that can predict the 3D surface of foam generation and the two steady-state strong-foam regimes. Following recent studies of Gauglitz *et al.* [2002], Kam and Rossen [2003], and Kam *et al.* [2004], this study aims to understand the mechanisms of foam displacement in porous media. By accounting for lamella mobilization and division induced by pressure gradient, this study fully accounts for the nonlinear relationship between the injection rate and pressure gradient, resulting from the interplay between the rates of lamella creation and coalescence. The results are compared with the catastrophic nature of foam rheology in porous media including three different foam states and the onset of foam generation (*cf.*, Fig. 2-9). More specifically, this study has the following objectives:

1. In line with the recent findings that "lamella mobilization and division" is the main mechanism of lamella creation, incorporate a new lamella-creation function that accounts for the pressure gradient for lamella mobilization into the framework of fractional flow theory and observe how three different foam states (weak-, intermediate- and strong-foam states) are delineated in the domain of f_w vs. S_w over a wide range of injection velocities.

2. The degree of gas-mobility reduction in the presence of foam is not independent of injection velocity. The change in injection velocity results in the change in gas viscosity, pressure gradient, foam texture and water saturation, which subsequently alters the rates of lamella creation and coalescence. Visualize these complicated velocity-dependent fractional flow curves in a 3D domain (f_w and S_w in x and y-axes and u_t in z axis) to capture how the nonlinear kinetics could affect fractional flow curves when the injection rate is varied.

3. Solve the new fractional flow curves with the method of characteristics and compare the results with relevant simulation studies in literature. Understand the significance of multi-valued foam-generation surface within the context of Buckley-Leverett solutions for immiscible displacements. Also evaluate the roles of fractional flow solutions as a mathematically robust

guide to the simulation studies of complicated displacement problems in porous media.

3. Methodology

For conventional gas-water two-phase flow, the fractional flow of water (f_w) is defined by

$$f_w = \frac{u_w}{u_t} = \frac{u_w}{u_g + u_w} \tag{3-1}$$

where f_w is the fractional flow of liquid phase, u_w and u_g are the volumetric fluxes of liquid and gas phases respectively, and u_t is total volumetric flux. For horizontal displacements with negligible capillary-pressure gradients, Eq. (3-1) becomes

$$f_w = \frac{1}{1 + \frac{\mu_w}{k_{rw}} \frac{k_{rg}}{\mu_g}} \tag{3-2}$$

where μ_w and μ_g are the viscosities of liquid and gas and k_{rw} and k_{rg} the relative permeabilities to liquid and gas phases respectively.

We use Corey-type relative permeability functions in which the coefficients and exponents are derived from data in Collins (1961), *i.e.*,

$$k_{rw} = 0.7888 \left(\frac{S_w - S_{wc}}{1 - S_{wc} - S_{gr}} \right)^{1.9575} \tag{3-3}$$

and

$$k_{rg} = \left(\frac{1 - S_w - S_{gr}}{1 - S_{wc} - S_{gr}} \right)^{2.2868} \tag{3-4}$$

where S_{wc} is connate water saturation and S_{gr} is residual gas saturation.

Both gas viscosity and gas relative-permeability function can be affected significantly by the presence of foam, whereas liquid relative-permeability function is unaffected by foam [Friedmann *et al.*, 1991; Bernard *et al.*, 1965; Sanchez *et al.*, 1989]. For the mechanistic description of in-situ lamella creation, we follow the expression of Kam *et al.* [2004], a modified version of

Kam and Rossen [2003], accounting for the pressure gradient (∇p) and water saturation (S_w) as follows:

$$r_g = C_g S_w (\nabla p)^m \tag{3-5}$$

where r_g is the rate of lamella creation, C_g and m are the model parameters and ∇p is the pressure gradient. Note that Eq. (3-5) is in line with the theory of "lamella mobilization and division" [Rossen and Gauglitz, 1990; Kam and Rossen, 2003]. On the other hand, foam coalescence is governed by P_c^* or S_w^*, *i.e.*,

$$r_c = C_c n_f \left(\frac{1}{S_w - S_w^*} \right)^n \quad \text{, if } S_w \geq S_w^* \tag{3-6}$$

where r_c is the rate of lamella coalescence and n_f the number of lamellae per unit volume of gas, and C_c and n model parameters. Note that r_c goes to infinity as S_w approaches S_w^*.

The interplay between lamella creation and coalescence determines the number of lamellae and hence governs the foam texture. By equating Eqs. (3-5) and (3-6), foam texture (n_f) at local steady state becomes

$$n_f = \left(\frac{C_g}{C_c} \right) (S_w - S_w^*)^n S_w (\nabla p)^m \text{, if } S_w \geq S_w^* \tag{3-7}$$

Once $S_w \leq S_w^*$, no lamellae can survive due to the lack of aqueous phase. Thus, $n_f = 0$.

For gas viscosity in the presence of foam (μ_g^f), we use the shear-thinning effective viscosity suggested by Hirasaki and Lawson [1985], that is,

$$\mu_g^{\,f} = \mu_g^{\,o} + \frac{C_f n_f}{u_g^{1/3}} \tag{3-8}$$

where μ_g^o is gas viscosity in the absence of foam and C_f is a model parameter accounting for gas viscosity in the presence of foam.

Darcy's law describes the flow of liquid and gas phases as

$$u_w = \frac{kk_{rw}\nabla p}{\mu_w} \tag{3-9}$$

and

$$u_g = \frac{kk_{rg}{}^{f}\nabla p}{\mu_g{}^{f}} \tag{3-10}$$

where k is absolute permeability, and $k_{rg}{}^{f}$ and $\mu_g{}^{f}$ the relative permeability and viscosity of gas phase in the presence of foam, respectively.

Since gas relative permeability and gas viscosity are often inseparable in the presence of foam, we include all foam effects, for simplicity, in the gas-viscosity term, *i.e.*,

$$u_g = \frac{kk_{rg}{}^{o}\nabla p}{\mu_g{}^{f}} \tag{3-11}$$

where $k_{rg}{}^{o}$ is gas relative permeability in the absence of foam. In local steady-state modelling, one can determine $\mu_g{}^{f}$ and u_g simultaneously solving Eqs. (3-8) and (3-10) and construct foam fractional curves using Eq. (3-2).

This foam model offers a successful fit to the three foam states (weak, intermediate and strong) and the two steady-state strong-foam regimes (low-quality and high-quality) observed in laboratory experiments [Alvarez *et al.*, 2001; Gauglitz *et al.*, 2002]. To comply with the fractional flow theory, we assume incompressible phases, immediate attainment of local steady state, and negligible capillary pressure gradient.

Algorithms for the construction of fractional flow curves are described in Appendix A with detailed explanations on the construction of saturation profile, effluent history, and time-distance diagram. An example of an Excel subroutine for the calculation of foam viscosity ($\mu_g{}^{f}$) and local superficial gas velocity (u_g) is given in Appendix B.

In one-dimensional dynamic foam simulations, two hyperbolic partial differential equations should be solved simultaneously: one, a mass balance

for either gas or liquid phase; and the other, bubble population balance for foam texture [Falls *et al.*, 1988; Friedmann *et al.*, 1991; Kovscek *et al.*, 1995; Bertin *et al.*, 1998; Kam *et al.*, 2004], *i.e.*,

$$\phi\frac{\partial S_j}{\partial t}+\frac{\partial u_j}{\partial x}=0\ ,\ i=water,gas \tag{3-12}$$

and

$$\phi\frac{\partial}{\partial t}\left(S_g n_f\right)+\frac{\partial}{\partial x}\left(n_f u_g\right)=R=\phi S_g\left(r_g-r_c\right) \tag{3-13}$$

where, t and x are time and space respectively. More details on foam simulation with ∇p-dependent lamella-creation mechanism can be found in Kam *et al.* [2004]. For foam simulation during gas injection in this study, Kam *et al.*'s [2004] simulation technique was further developed to obtain better numerical convergence and stability.

4. Results and Discussions

Once constructed, a fractional flow curve can be solved with given initial and injection conditions. In all cases studied (otherwise noted), the initial condition is a porous medium fully saturated with surfactant solution (S_w = 1) and the injection condition is co-injection of gas and surfactant solution at fixed u_t keeping f_g = 0.72 (or f_w = 0.28 equivalently). This particular set of initial and injection conditions allows comparisons between the analytical solutions in this study and the simulation results available in Kam *et al.* [2004]. Model parameters are as follows: k = 30 μm^2, S_w^* = 0.0585, μ_w = 0.001 Pa·s, μ_g = 0.00002 Pa·s, ϕ = 0.31, S_{wc} = 0.04, S_{gr} = 0, C_g = 15548.8, C_c = 0.1, m = 2.4, n = 0.28 and $C_f = 1 \times 10^{16}$ and $n_f^{max} = 8 \times 10^{13}$ m^{-3}.

Fig. 4-1 shows the fractional flow curve for gas-water flow in the absence of foam constructed from Eqs. (3-2), (3-3) and (3-4). "I" and "J" represent the initial and injection conditions. The slope at any saturation on the f_w-S_w curve (*i.e.*, df_w/dS_w) represents the dimensionless velocity of a wave at that particular saturation. Discontinuity in S_w (or, a shock) occurs when the rearward waves of higher velocities overtake the forward waves of lower velocities [Lake, 1989]. As a result, the velocity should always increase monotonically from "J" to "I". As graphically demonstrated in Fig. 4-1, there is a shock from "I (S_{wI}, f_{wI})" to shock front "(S_{wf}, f_{wf})" followed by spreading waves to "J (S_{wJ}, f_{wJ})".

Fig. 4-2 shows the solutions to the fractional flow curve (*cf.*, Fig. 4-1) in terms of water saturation and pressure profile. Fig. 4-2a shows that there is a discontinuity in S_w at the leading edge of the gas bank which is followed by gradual reduction (or, spreading waves) in S_w until S_w reaches S_{wJ}. Corresponding pressure profile is shown in Fig. 4-2b, calculated by Darcy's equations given in Eqs. (3-9) and (3-10).

Fig. 4-3 shows the case of simultaneous injection of gas and surfactant solution at u_t = 1.02 ft/day. At this low u_t, the fractional flow curve is analogous to that of gas-water flow (*cf.*, Fig. 4-1) except for the isolated loop at low S_w (*i.e.*, the dotted line with circular symbols). This means that, for the case shown in Fig. 4-3, the injection condition of $0.35 < f_w < 0.89$ has triple solutions: the lowest S_w for strong foam (left-hand side of the loop), the highest S_w for weak foam, and S_w in between for foams in the intermediate state (right-

hand side of the loop). Once the maximum foam texture n_f^{max} is incorporated into the model, the entire loop at low S_w vanishes and is replaced by a new path (*i.e.,* the solid line with triangular symbols next to the loop in Fig. 4-3). This implies that the solutions represented by the loop are wholly imaginary and, if strong foam ever exists, it should be at its minimum bubble size [Rossen and Wang, 1999; Alvarez *et al.*, 2001]. Injected foam quality of f_g = 0.72 (*cf.,* dashed line in horizontal direction in Fig. 4-3) provides the location of "J" which, in this case, falls on weak-foam state. Similar to the case of gas-water displacement (*cf.,* Fig. 4-1), a shock and spreading waves from "I" to "J" are observed

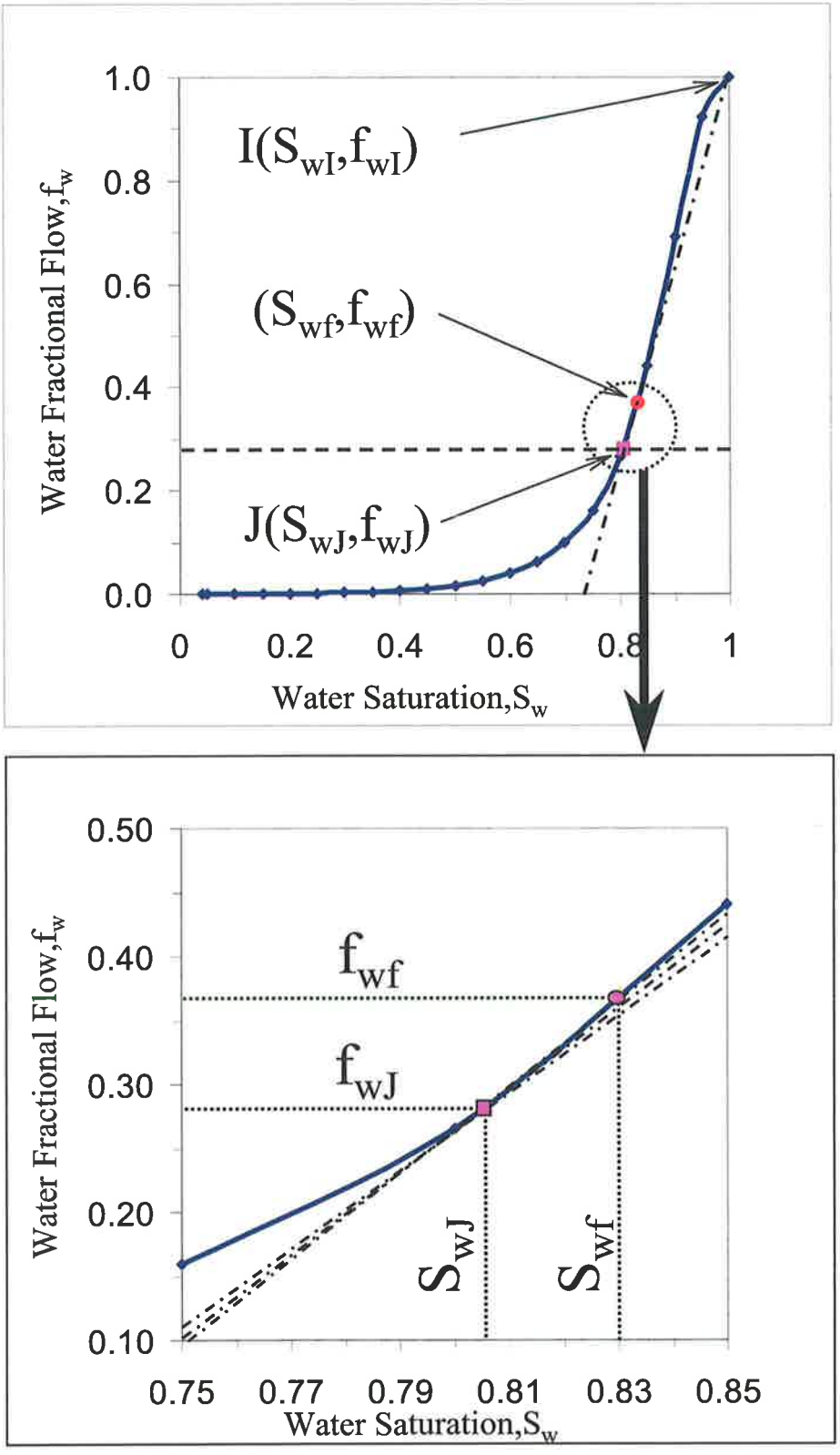

Fig. 4-1. Fractional flow curve for conventional gas-water flow: a shock from "I" to (S_{wf},f_{wf}) followed by spreading waves to "J".

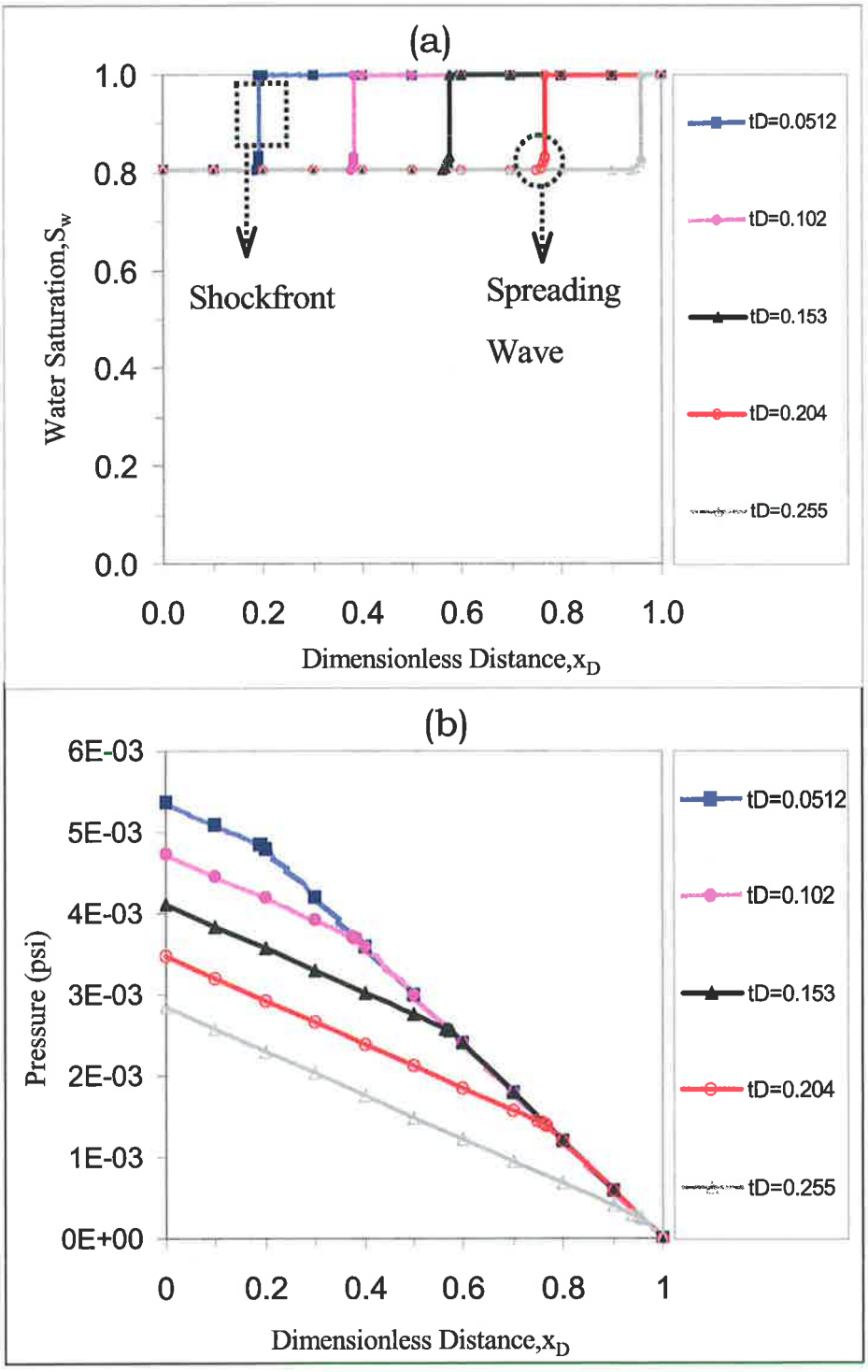

Fig. 4-2. Solution to the gas-water fractional flow curve (*cf.*, Fig. 4-1): (a) Saturation profile and (b) Pressure profile (t_D represents dimensionless time in the unit of pore volume injected).

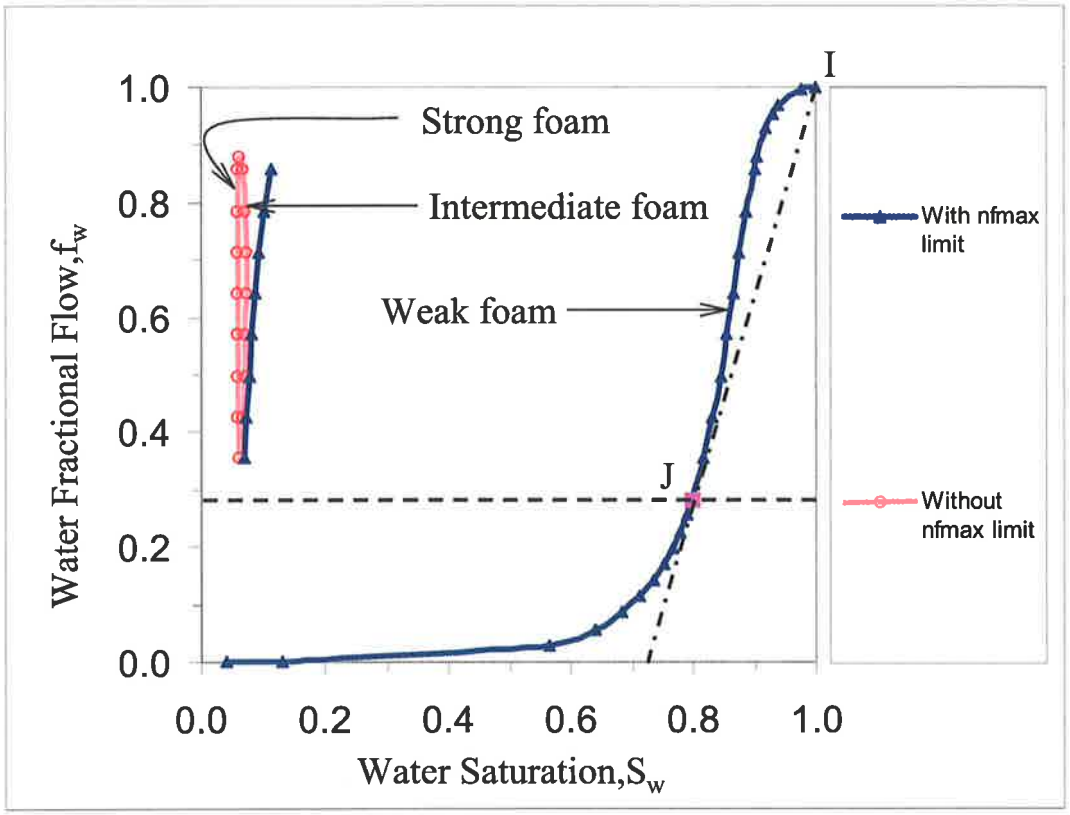

Fig. 4-3. Foam fractional flow curve at u_t = 1.02 ft/day: at the given injection condition (f_g = 0.72), there is only one solution in the weak-foam state.

Fig. 4-4 shows the saturation profile predicted by the fractional flow curve (Fig. 4-4a; *cf.*, Fig. 4-3) compared with the simulation results in Kam *et al.*'s [2004] study (Fig. 4-4b). Although the simulation results with 25 grid blocks show some numerical dispersion, not only the average velocity of the foam front but also the saturation behind the shock is well captured by the fractional flow solution. Simulations at much finer grid system, in fact, show good agreement between the two, including the behaviours at the shock and spreading waves (not shown). Because the fractional flow theory offers an analytical solution, it is not affected by the numerical dispersion.

Fig. 4-5 shows the foam texture predicted by the fractional flow curve (Fig. 4-5a; *cf.*, Fig. 4-3) compared with that in the simulation study (Fig. 4-5b). The scales in the y-axes are identical for comparison. Foam texture behind the shock in the fractional flow solution is in good agreement with that in the simulation. It should be noted that the peak in n_f in the simulation is caused by the dynamic nature of lamella creation and coalescence as gas and surfactant solution enter the next grid block in fully mechanistic foam simulations. This study does not intend to fit such dynamic mechanisms, nor is the fractional flow theory capable of handling such transient behaviours. In other words, the fractional flow solution is a quasi-static model assuming that the system reaches local equilibrium states instantaneously during the flow of gas and surfactant solution. It should also be pointed out that the magnitude of the peaks and the width of leading-edge of foam front in the dynamic simulation depend strongly on the numerical artefact such as grid-block size and time step.

Fig. 4-6 shows the pressure profile from the fractional flow curve (Fig. 4-6a; *cf.*, Fig. 4-3) compared with that in the simulation study (Fig. 4-6b). They are in good agreement. In comparison with the case of gas-water displacement (*cf.*, Fig. 4-2), there is a slight increase in the pressure gradient resulting from the propagation of weak foam in the media.

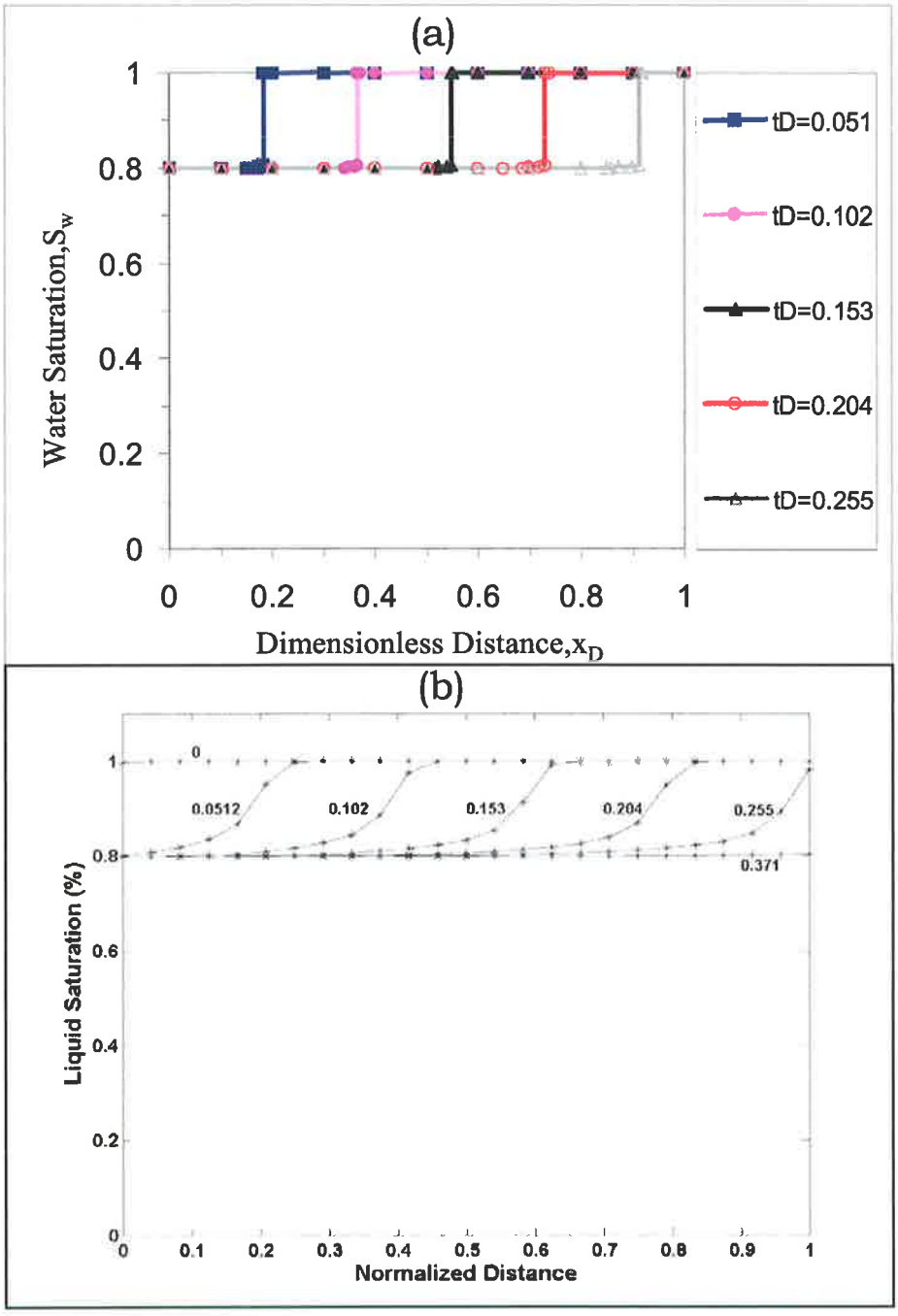

Fig. 4-4. Comparison between (a) fractional flow solution and (b) simulation [Kam *et al.*, 2004] in terms of saturation profile at u_t = 1.02 ft/day and f_g = 0.72 (*cf.*, Fig. 4-3).

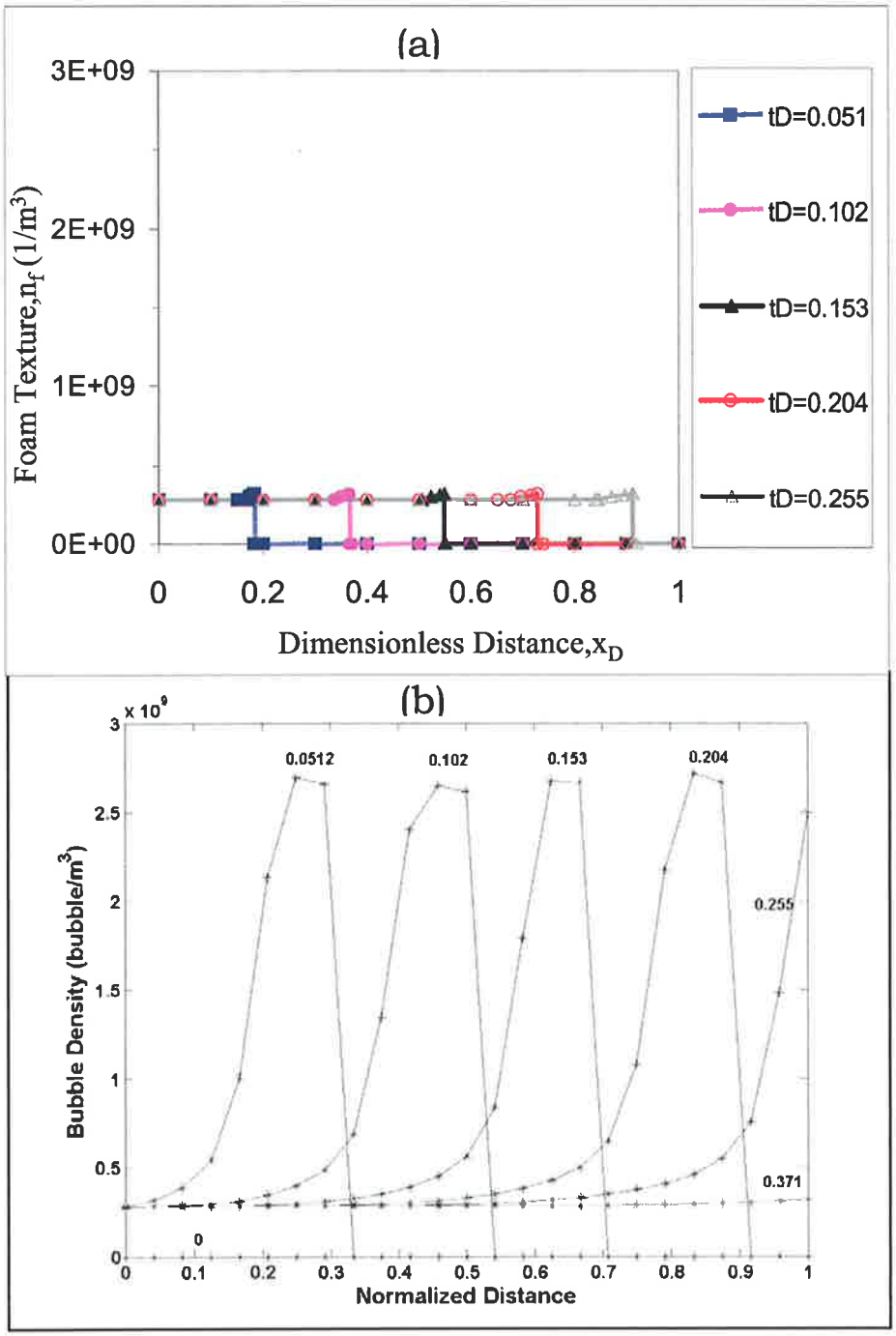

Fig. 4-5. Comparison between (a) fractional flow solution and (b) simulation [Kam *et al.*, 2004] in terms of foam texture profile at u_t= 1.02 ft/day and f_g = 0.72 (*cf.*, Fig. 4-3).

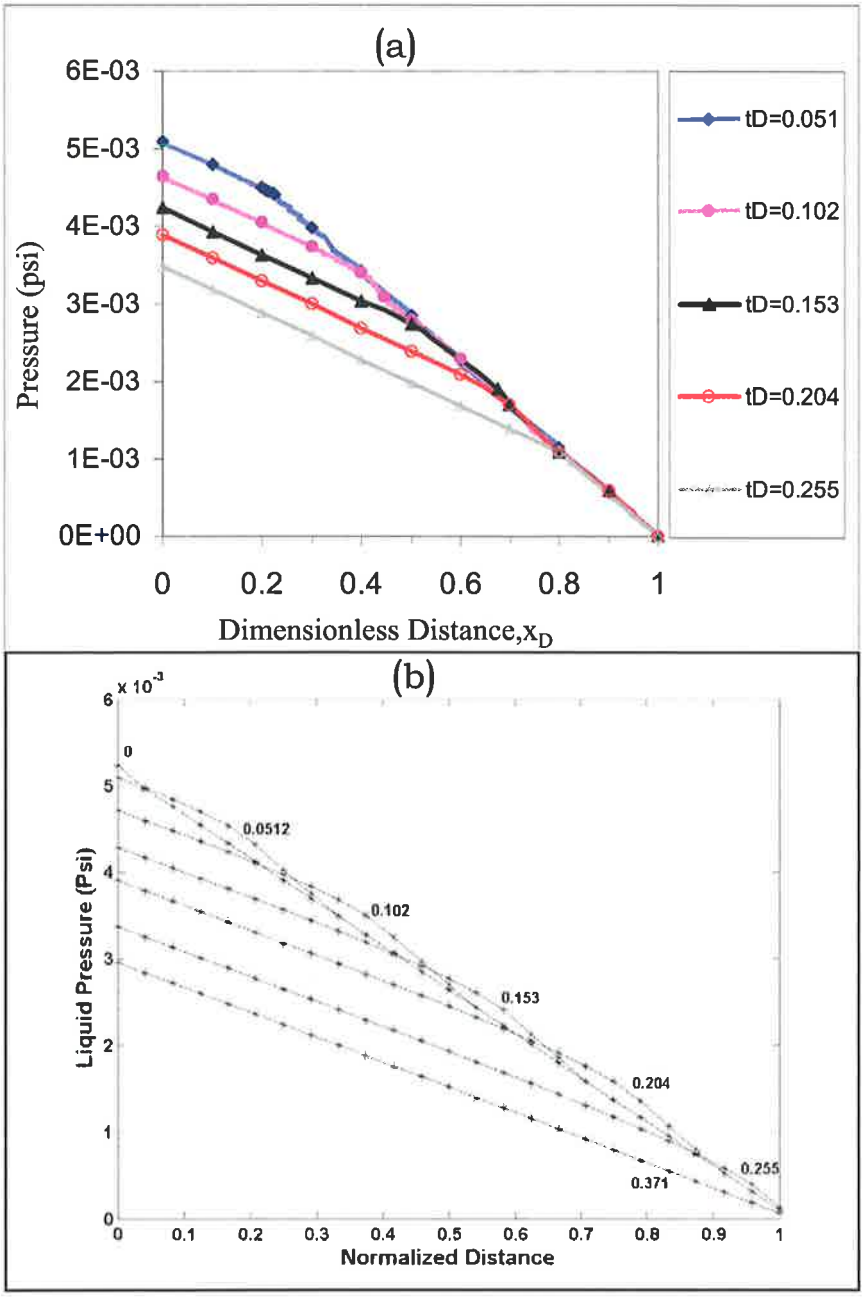

Fig. 4-6. Comparison between (a) fractional flow solution and (b) simulation [Kam *et al.*, 2004] in terms of pressure profile at u_t = 1.02 ft/day and f_g = 0.72 (*cf.*, Fig. 4-3).

Fig. 4-7 shows the fractional flow curves in simultaneous injection of gas and surfactant solution at u_t = 8.31 ft/day, approximately 8.15 times higher than that in Fig. 4-3. The formation of strong foam at high u_t reduces S_w significantly and, as a result, three different foam states appear in a narrower range of f_w (*i.e.,* 0.032 < f_w < 0.16). Similar strange-shaped fractional flow curves were observed and studied by others [Kibodeaux and Rossen, 1997; Wassmuth *et al.*, 2001; Rossen and Bruining, 2004]. Injected foam quality of f_g = 0.72, as shown by the horizontal dashed line in Fig. 4-7, has only one intersection ("J" in Fig. 4-7) with the fractional flow curve. Such a change in the fractional flow curve is consistent with existing knowledge in that coreflooding experiments at sufficiently high injection velocities result in strong foam propagation. Similar to the case in Fig. 4-3, the use of n_f^{max} makes the curve shift slightly to higher S_w. It is worth noting that the almost vertical part of the fractional flow curve (*i.e.,* 0.032 < f_w < 0.10 near S_w^*) corresponds to strong foam in the high-quality regime in which foam stability is governed by bubble coalescence and n_f is always less than n_f^{max}. When f_w reaches 0.10 approximately, n_f reaches n_f^{max} and foam rheology starts to be dominated by bubble trapping and mobilization, which is typical of strong foam in the low-quality regime. This implies that the shock wave from "I" to "J" in the presence of strong foam in Fig. 4-7 has foam texture of n_f^{max} right behind the foam front. Fig. 4-7 also explains why foam generation is more difficult with drier foam. Although f_g = 0.72 corresponds to strong-foam propagation, higher f_g can lead to weak-foam propagation.

Fig. 4-8 compares the saturation profile for strong foam from the fractional flow curves with that in the simulation. Both results consistently show that the water saturation behind the shock is approximately at S_w = 0.075. The location of displacement front is also well captured even though the front in the simulation tends to spread out slightly due to numerical dispersion.

Fig. 4-9 shows the change in foam texture. As shown in Fig. 4-7, the initial condition is followed by a shock which is identical to the injection condition. Further, the conditions behind the shock fall into the strong-foam state in the low-quality regime and thus $n_f = n_f^{max}$. Both the fractional flow solution and simulation results show consistency in that n_f = 0 ahead of the shock and $n_f = n_f^{max}$ behind the shock.

Fig. 4-10 is the comparison between the fractional flow solution and simulation in terms of the pressure profile. Both results show good agreement. Note that the pressure gradient of strong foam in Fig. 4-10 is more than 3000 times higher than that of weak foam in Fig. 4-6, which results from the increase of foam texture by more than five orders of magnitude (*cf.*, Figs. 4-5 and 4-9).

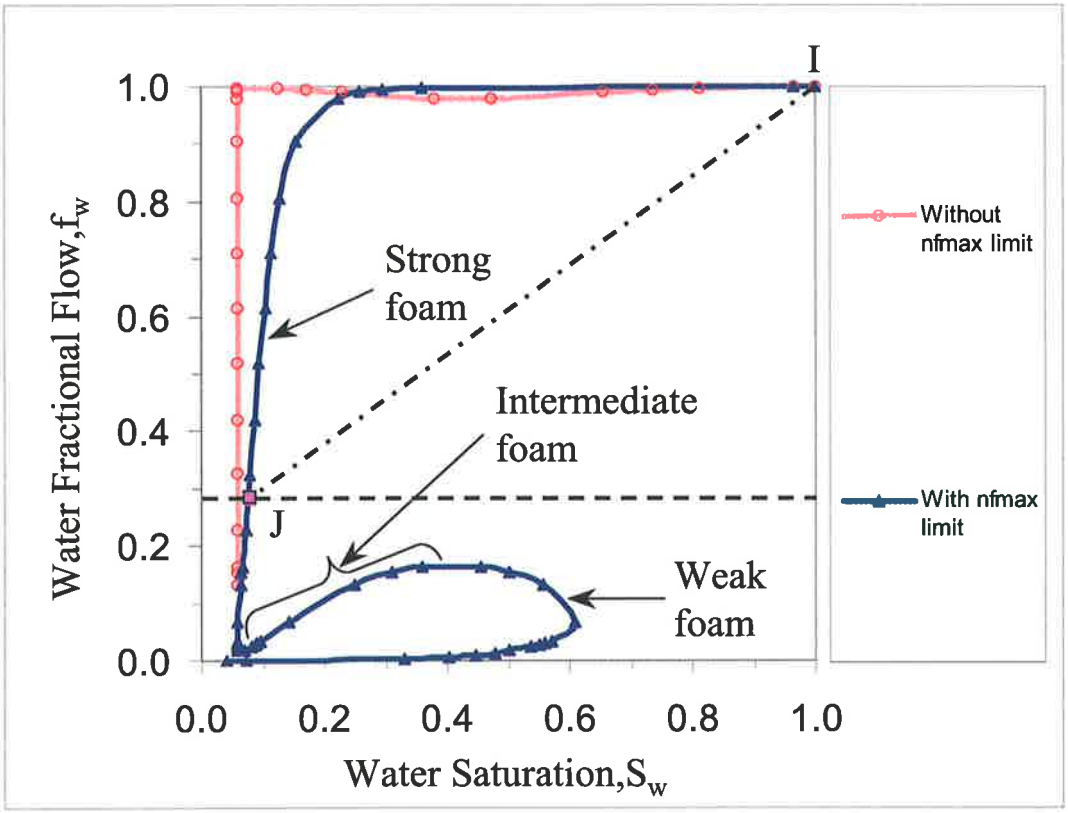

Fig. 4-7. Foam fractional flow curve at u_t = 8.31 ft/day: at the given injection condition (f_g = 0.72), there is only one solution in the strong-foam state.

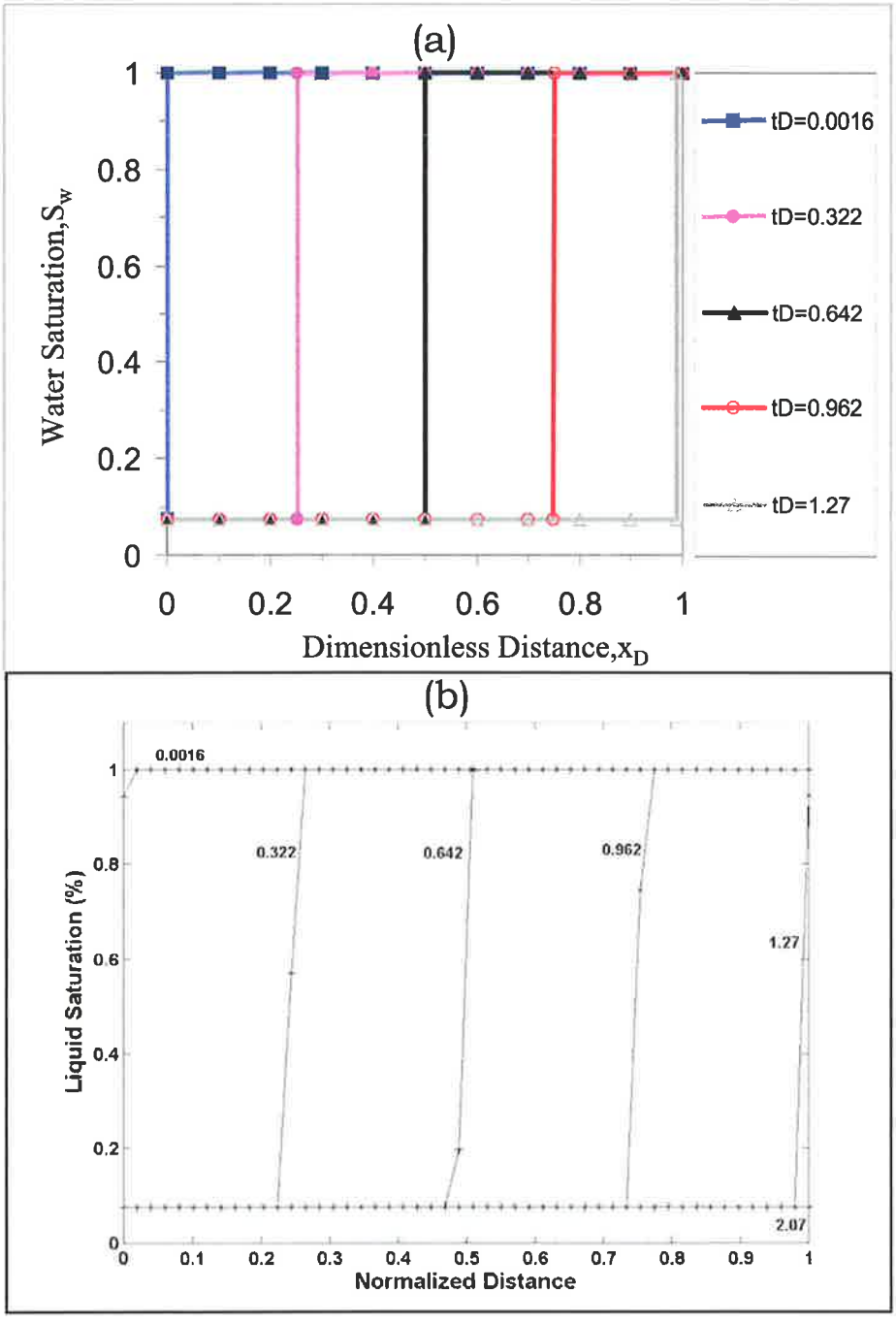

Fig. 4-8. Comparison between (a) fractional flow solution and (b) simulation [Kam *et al.*, 2004] in terms of saturation profile at u_t = 8.31 ft/day and f_g = 0.72 (*cf.*, Fig. 4-7).

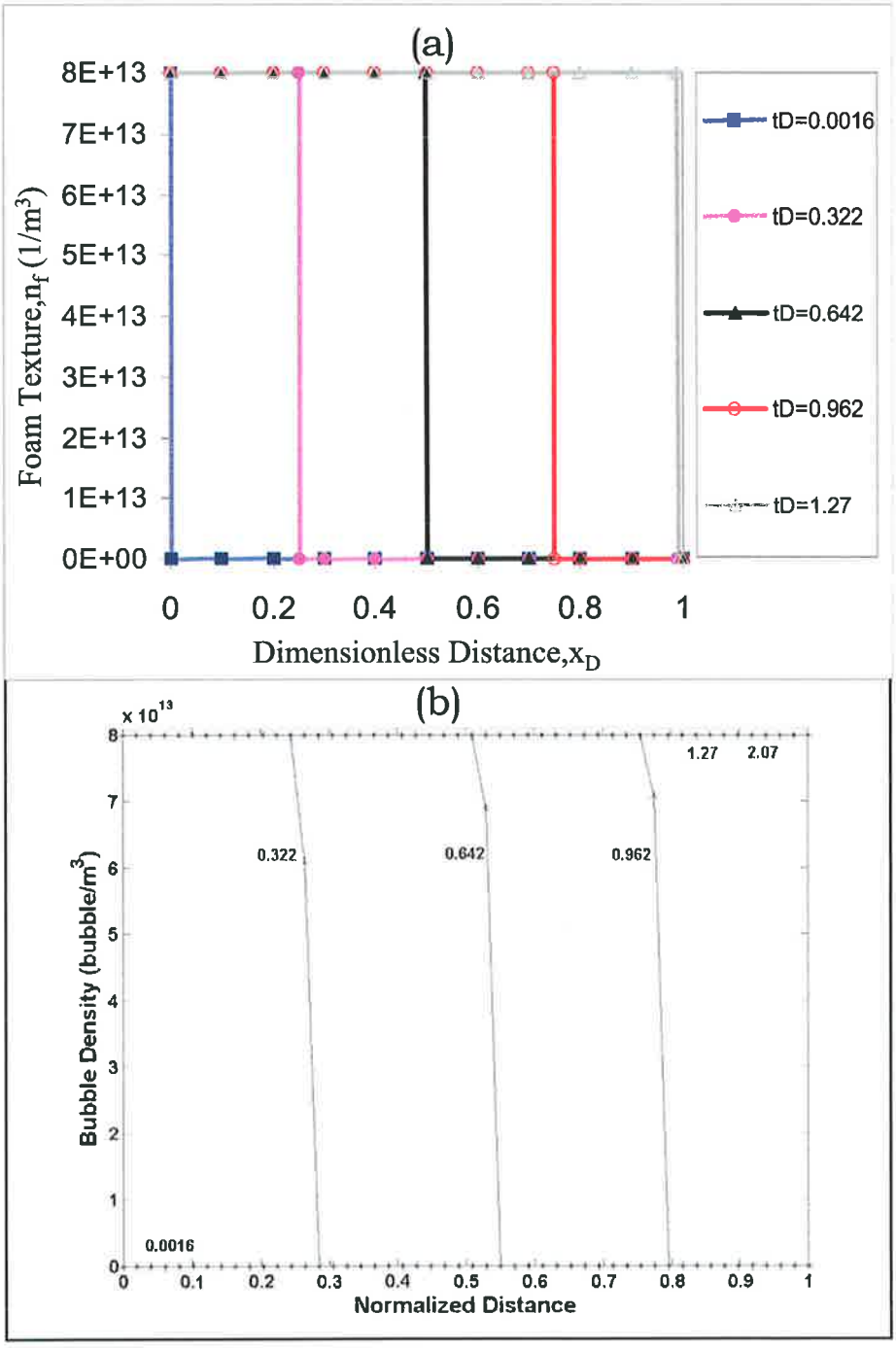

Fig. 4-9. Comparison between (a) fractional flow solution and (b) simulation [Kam *et al.*, 2004] in terms of foam texture profile at u_t = 8.31 ft/day and f_g = 0.72 (*cf.*, Fig. 4-7).

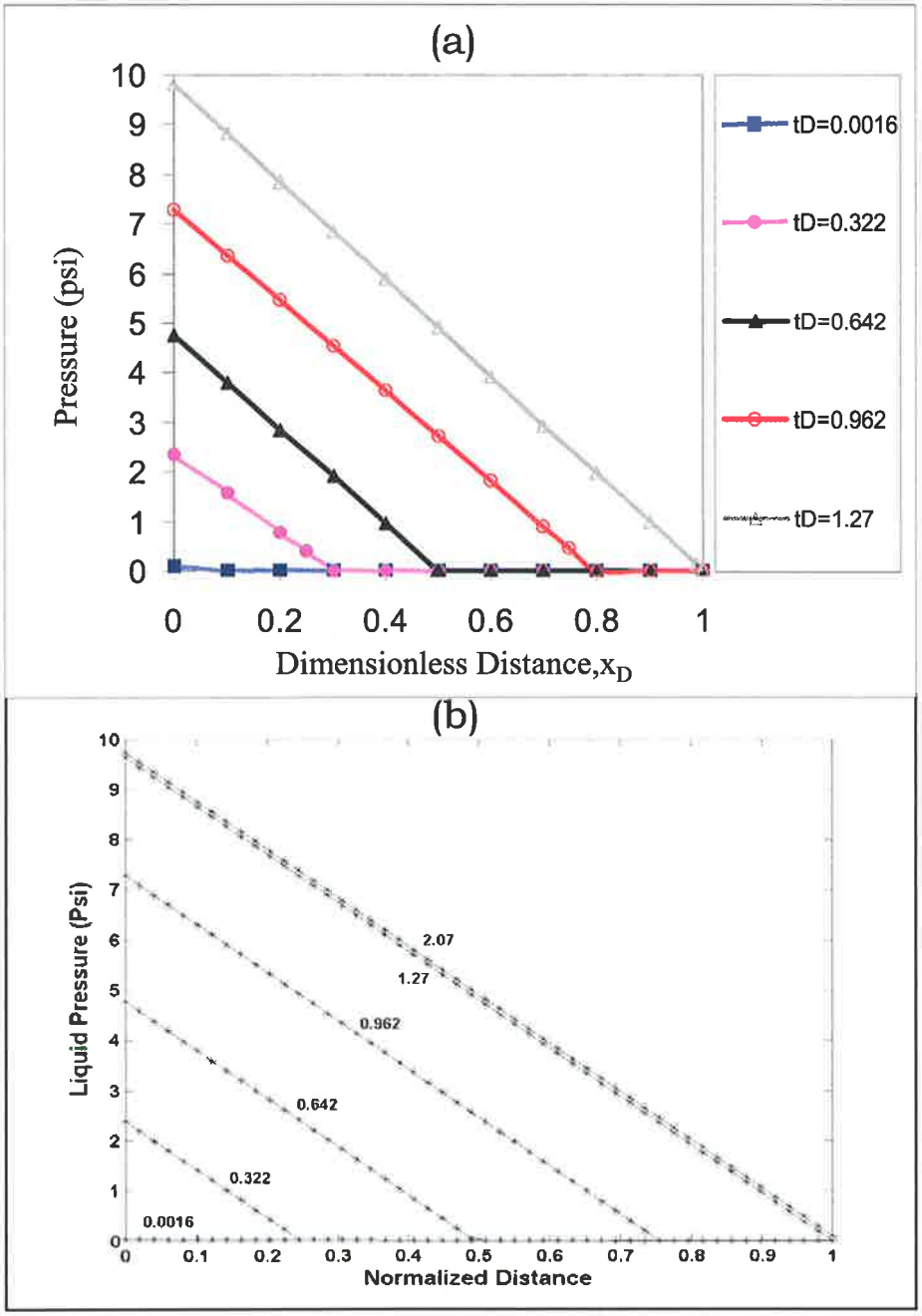

Fig. 4-10. Comparison between (a) fractional flow solution and (b) simulation [Kam *et al.*, 2004] in terms of pressure profile at u_t = 8.31 ft/day and f_g = 0.72 (*cf.*, Fig. 4-7).

Fig. 4-11 shows the fractional flow curves at intermediate injection velocities of u_t at 2.91 and 4.91 ft/day, in between those in weak-foam (*cf.*, Fig. 4-3) and strong-foam (*cf.*, Fig. 4-7). At the given injection foam quality, both cases exhibit triple solutions: "J_1" and "J_3" for weak- and strong-foam states and "J_2" in intermediate foam state. It should be noted that not all three graphical solutions ("J_1", "J_2", and "J_3") as shown in Fig. 4-11 are physically meaningful due to two reasons: firstly, the stability analysis shows that, at fixed u_t and f_g foam displacement, the intermediate state is unstable and thus the system spontaneously moves towards either weak-foam or strong-foam state [Kam *et al.*, 2004]. Therefore "J_2 " in Fig. 4-11 cannot be the solution. Secondly, any portion that has a negative slope along the fractional flow curve (*i.e.*, $df_w/dS_w < 0$) is mathematically true but physically invalid [Rossen and Bruining, 2004] and, as a result, should not be accounted for in the fractional flow solutions. The former is the constraint specifically associated with the stability of dynamic foam displacements and the latter comes from the instability of the fractional flow analysis.

Fig. 4-11a is the case that the slope, df_w/dS_w, at "J_1" is very close to infinity, though still positive, such that a slight increase in u_t makes the slope negative. Therefore, "J_1" in this case can be a solution leading to weak-foam propagation. Fig. 4-11a also shows that there is another solution at low S_w, resulting in strong foam. Additional computer simulations performed in this study, similar to Kam *et al.* [2004], show that the final solution strongly depends on the initial condition of the core (not shown). When the core is initially saturated with water in the absence of foam (*cf.*, "I" in Fig. 4-11a), the simulation leads to weak foam at steady state. In contrast, when the initial condition is close to the strong-foam state with fine foam texture at low S_w, the simulation predicts strong foam at steady state. The fractional flow curve in Fig. 4-11a shows that both are equally achievable.

Fig. 4-11b shows that further increase in u_t causes the slope at "J_1" to be negative. As a result, there is only one solution available, shown by "J_3". It is clear that, if the injection velocity increased in a stepwise manner, foam generation would occur between Figs. 4-11a and 4-11b in actual laboratory coreflood experiments.

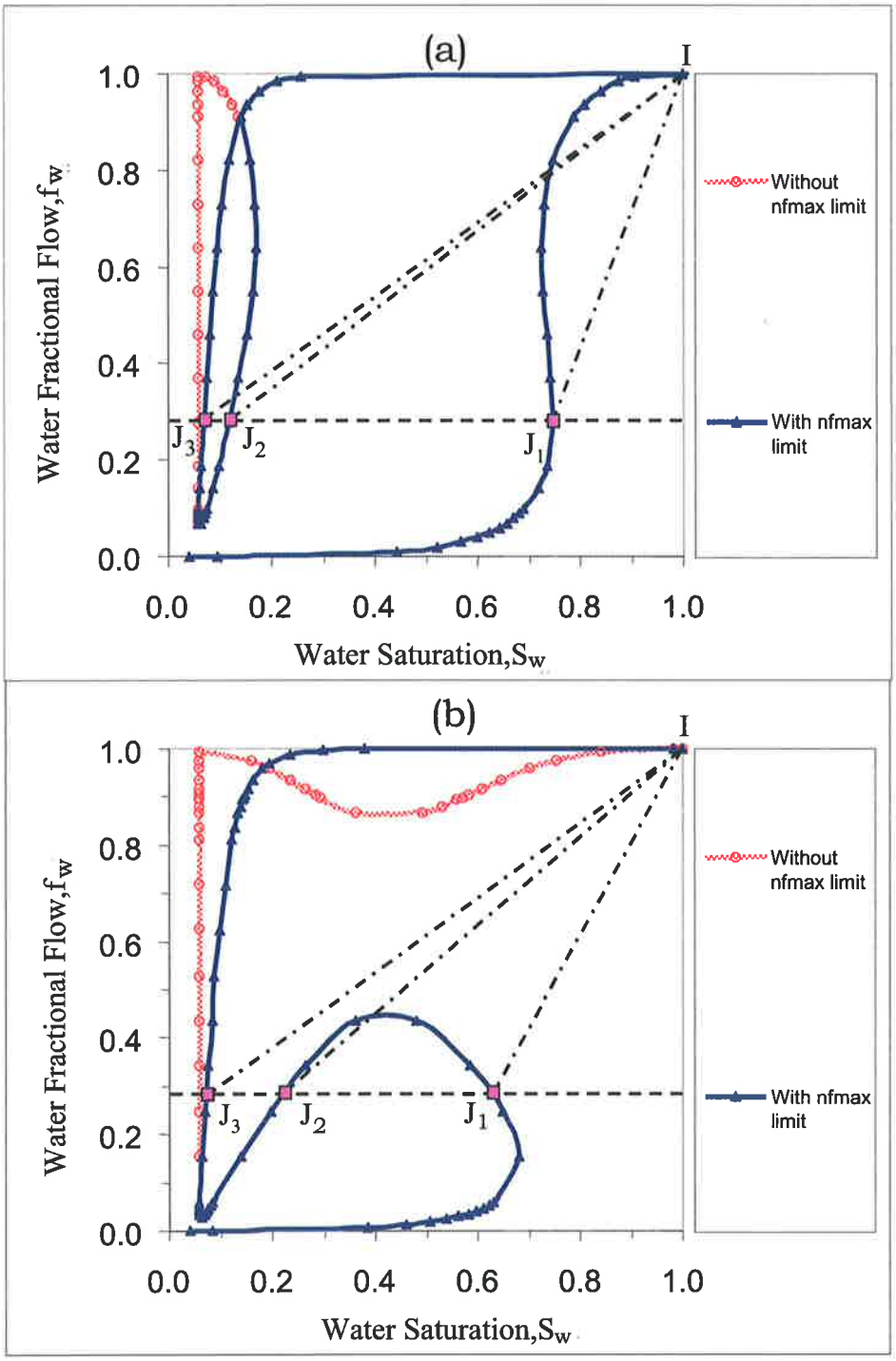

Fig. 4-11. Fractional flow curves at two intermediate values of u_t: (a) u_t = 2.91 ft/day and (b) u_t = 4.91 ft/day. Not all points that intersect the fractional flow curves are the actual solutions.

Fig. 4-12 shows the pressure profiles for the two cases shown in Fig. 4-11. As expected, sweep efficiency is greatly enhanced by the transition from weak-foam to strong-foam states. Fig. 4-13 shows the corresponding change in foam texture.

Fig. 4-14 shows a series of fractional flow curves in a wide range of injection velocities. Each figure consists of the fractional flow curves without and with n_f^{max} constraint (*i.e.*, dotted lines with circular symbols and solid lines with triangular symbols, respectively). The tendency of strong foam at high u_t (Figs. 4-14c through 4-14f) and weak foam at low u_t (Figs. 4-14a and 4-14b) at fixed f_g agrees well with the theory of foam generation. Fig. 4-14 also depicts how to explain the hysteresis in foam-generation experiments: the transition from weak-foam to strong-foam state would happen between (b) and (c) but the transition from strong-foam to weak-foam state would not occur even in Fig. 4-14a. However, once u_t is reduced significantly as shown in Fig. 4-3, foam coalescence can be observed. As a result, the transition from weak-foam to strong-foam state takes place at a higher u_t than the transition from strong-foam to weak-foam state.

Fig. 4-15 shows a 3D surface of fractional flow curves constructed from Figs. 4-3, 4-7 and 4-14 with u_t in z-axis. The portion that corresponds to $n_f > n_f^{max}$ is discarded. Construction of a 3D surface enables us to obtain a foam fractional flow curve at any particular u_t by slicing the surface along the horizontal plane.

In many foam applications, the steady-state pressure gradient is of great importance prior to the design of lab-scale and field-scale treatments. Fig. 4-16 shows the behavioural trend of pressure gradient at six different u_t values studied in Figs. 4-3, 4-7 and 4-14. As shown in Fig. 4-17, one can construct similar 3D surface with f_w, u_t, and steady-state ∇p in x-, y-, and z-axes, respectively. This 3D surface provides a means of conveniently relating u_t and f_g to ∇p.

The results in Fig. 4-3 through 4-17 show that the shape of fractional flow curves, displacement efficiency, and foam rheology are altered significantly when u_t changes by about 8.15 times (from u_t = 1.02 ft/day in Fig. 4-3 to u_t = 8.31 ft/day in Fig. 4-7). Quantitative description of the mechanisms of foam propagation in porous media cannot be obtained without having proper

mechanistic foam functions. It is also important to note that the key to the mechanistic description of foam behaviour is foam texture [*cf.*, Eq. (3-7)] that results from the mechanisms of lamella creation and coalescence [*cf.*, Eqs. (3-5) and (3-6)] .

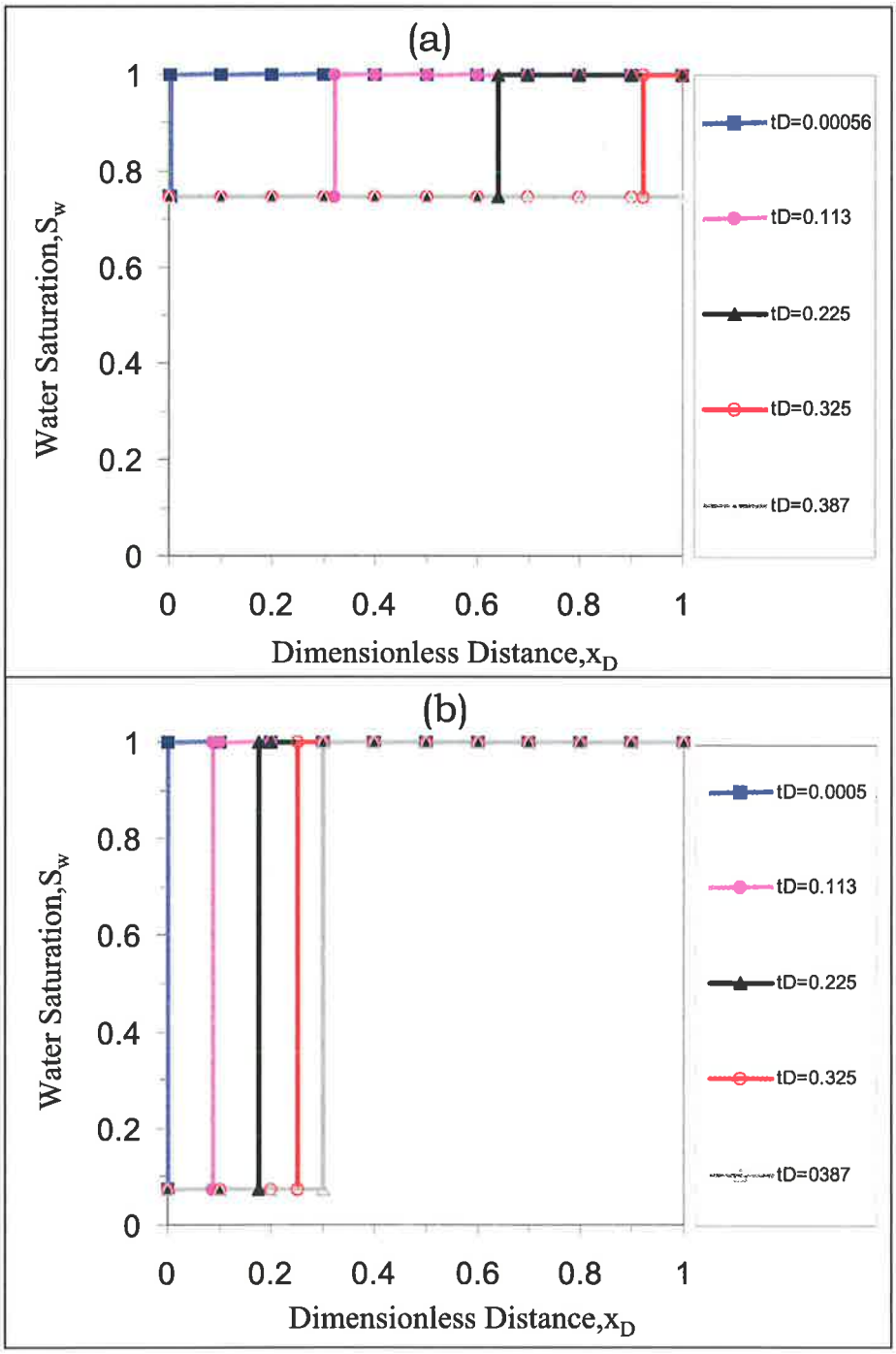

Fig. 4-12. Saturation profiles at two intermediate values of u_t: (a) u_t = 2.91 ft/day and (b) at u_t = 4.91 ft/day.

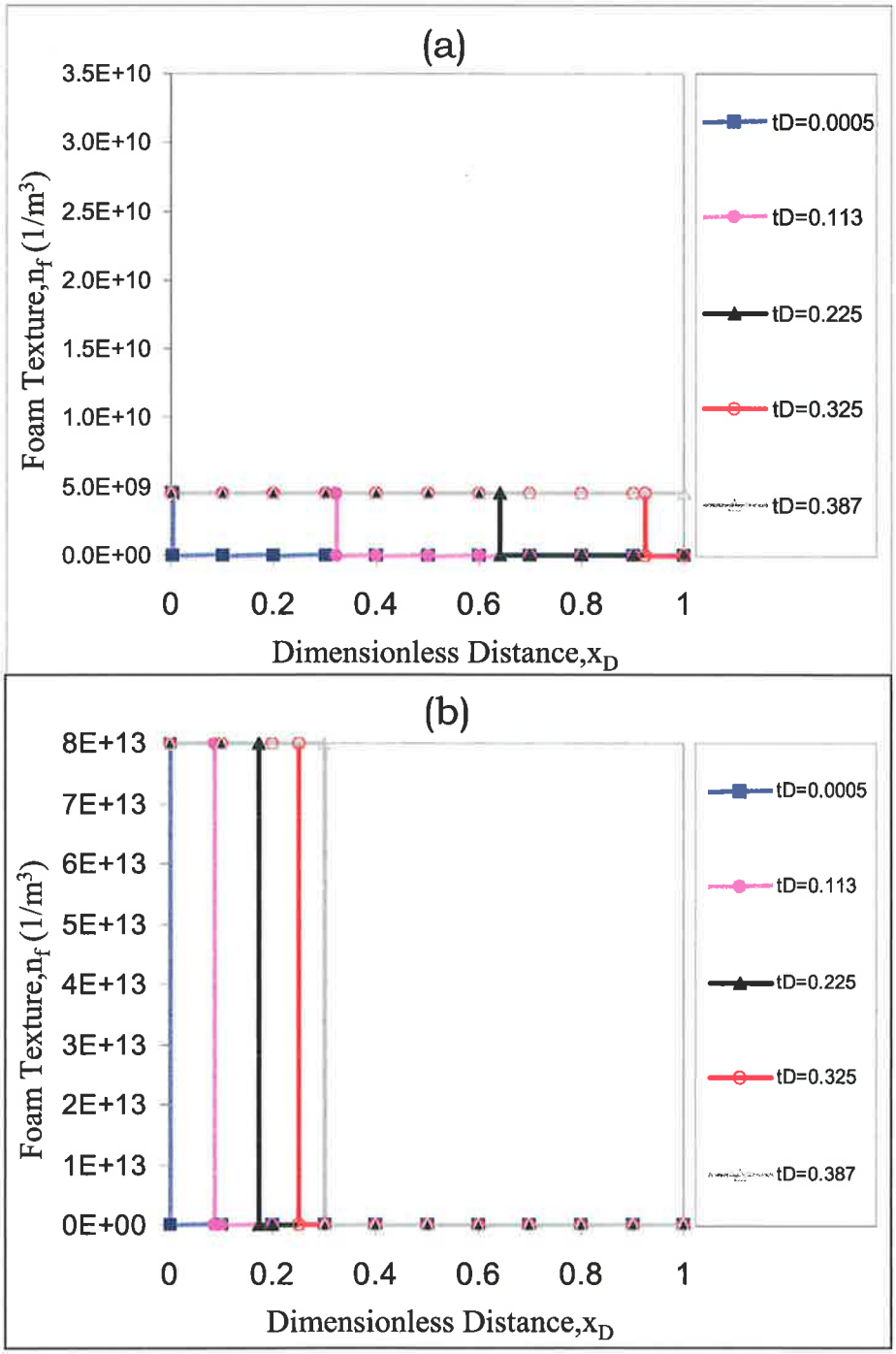

Fig. 4-13. Foam texture profiles at two intermediate values of u_t: (a) u_t = 2.91 ft/day and (b) u_t = 4.91 ft/day.

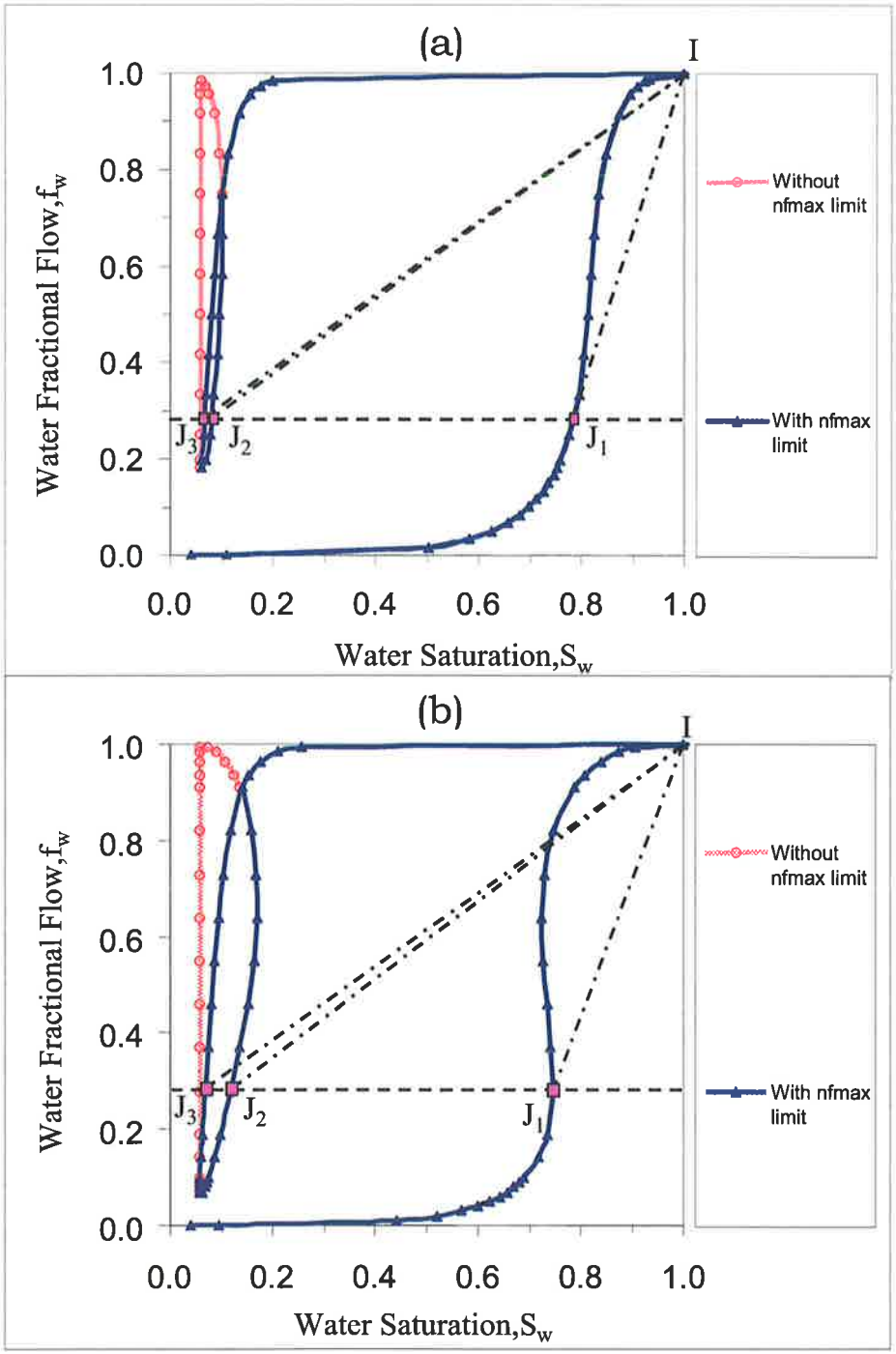

Fig. 4-14. Change in fractional flow curves as a function of u_t: (a) u_t = 1.72 ft/day (b) u_t = 2.91 ft/day.

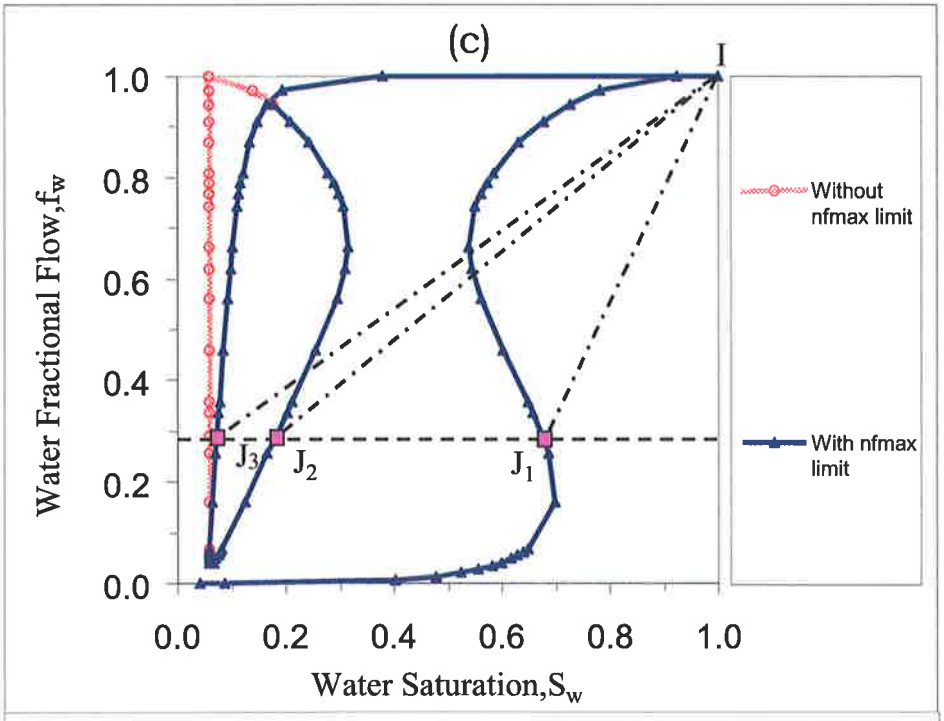

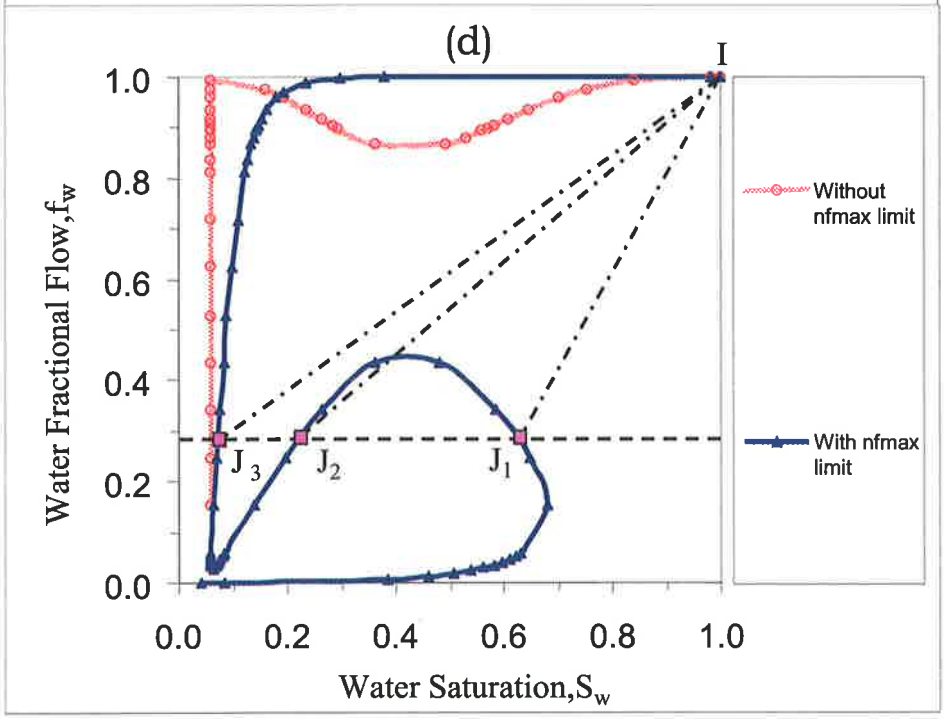

Fig. 4-14. Change in fractional flow curves as a function of u_t (continued): (c) u_t = 4.2 ft/day (d) u_t = 4.91 ft/day.

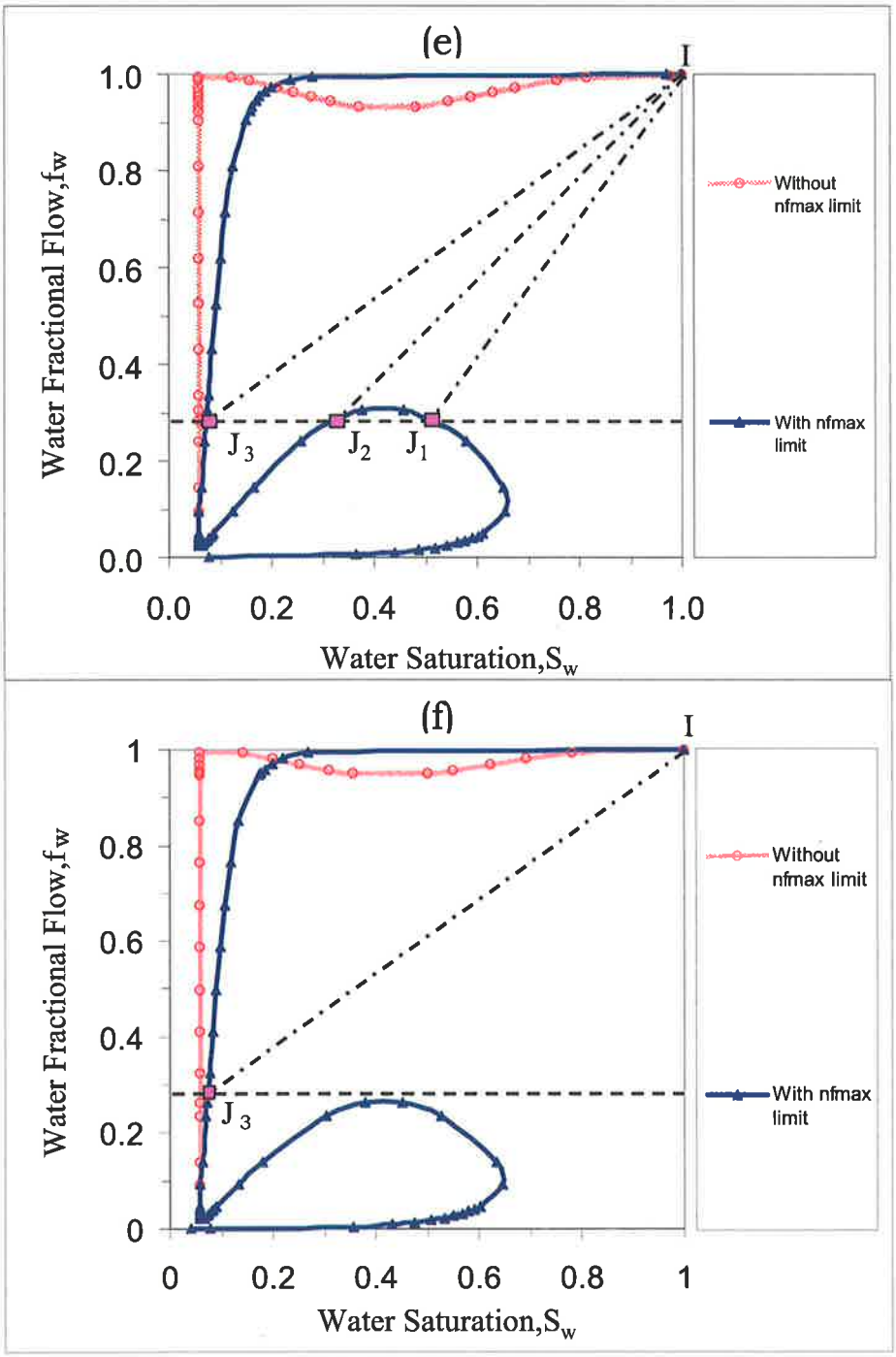

Fig. 4-14. Change in fractional flow curves as a function of u_t (continued): (e) u_t = 5.89 ft/day (f) u_t = 6.37 ft/day.

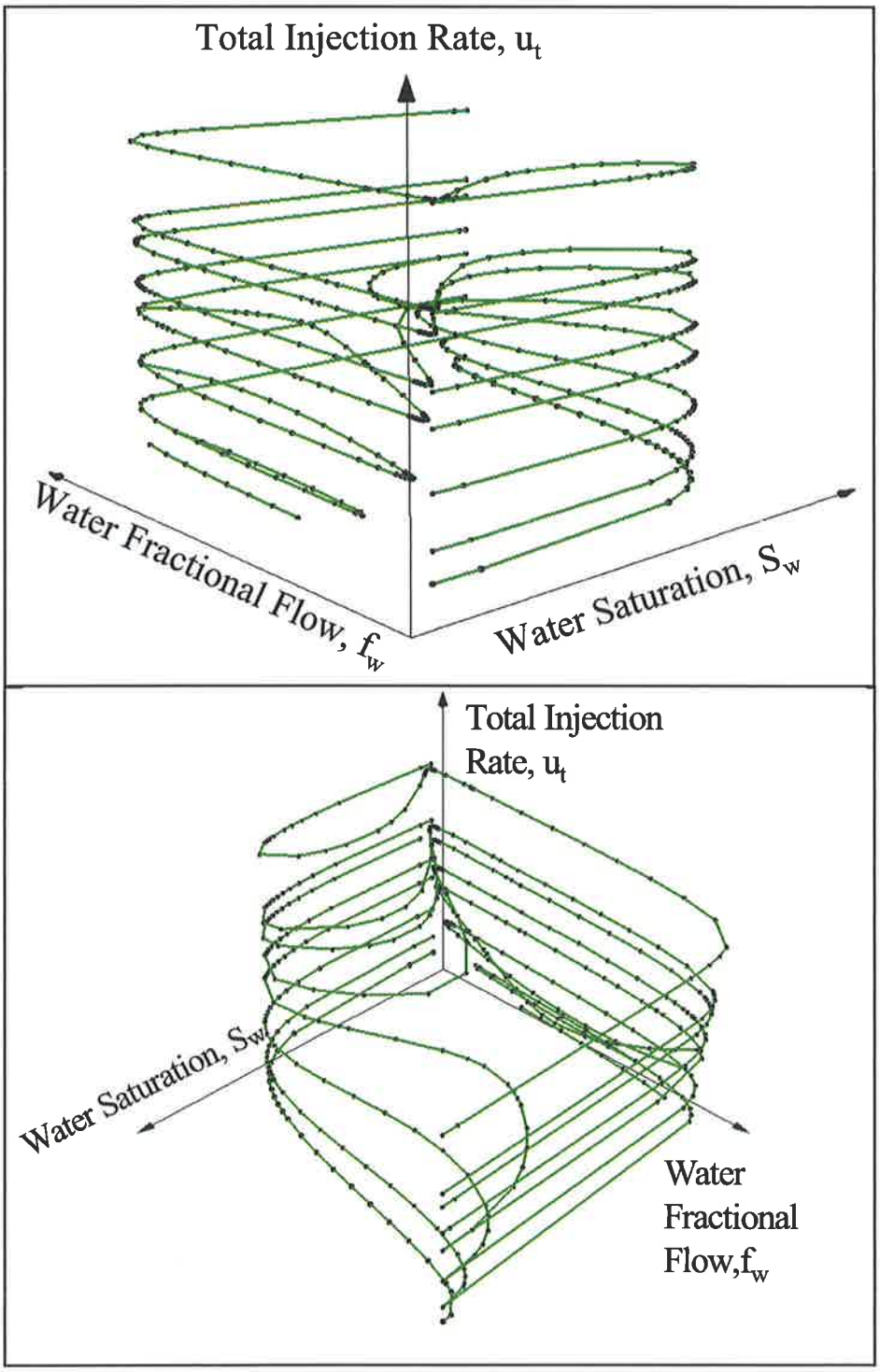

Fig. 4-15. Three dimensional surface of fractional flow curves at different values of total injection rate (u_t).

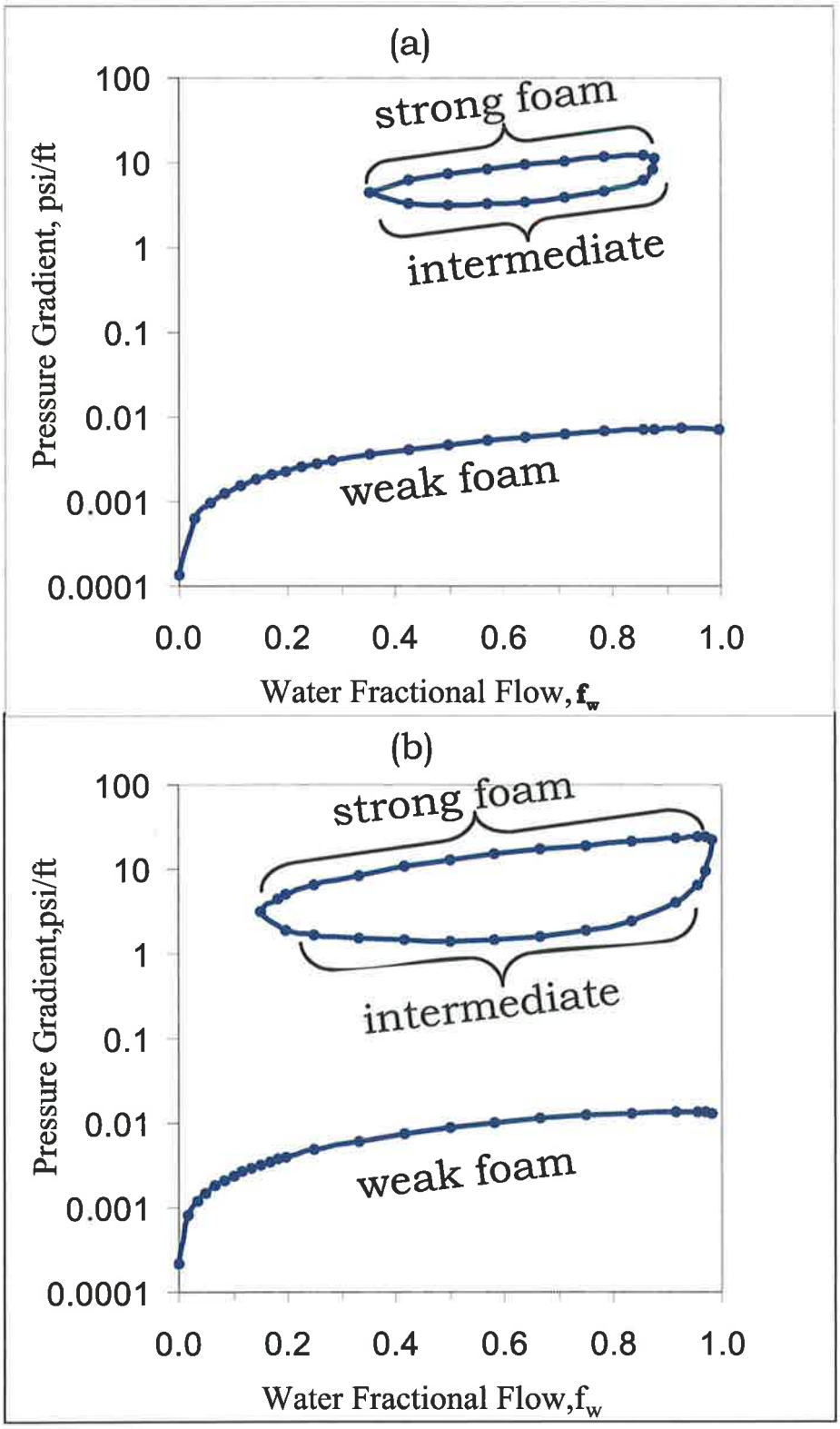

Fig. 4-16. Pressure gradient as a function of u_t: (a) u_t = 1.02 ft/day (b) u_t = 1.72 ft/day.

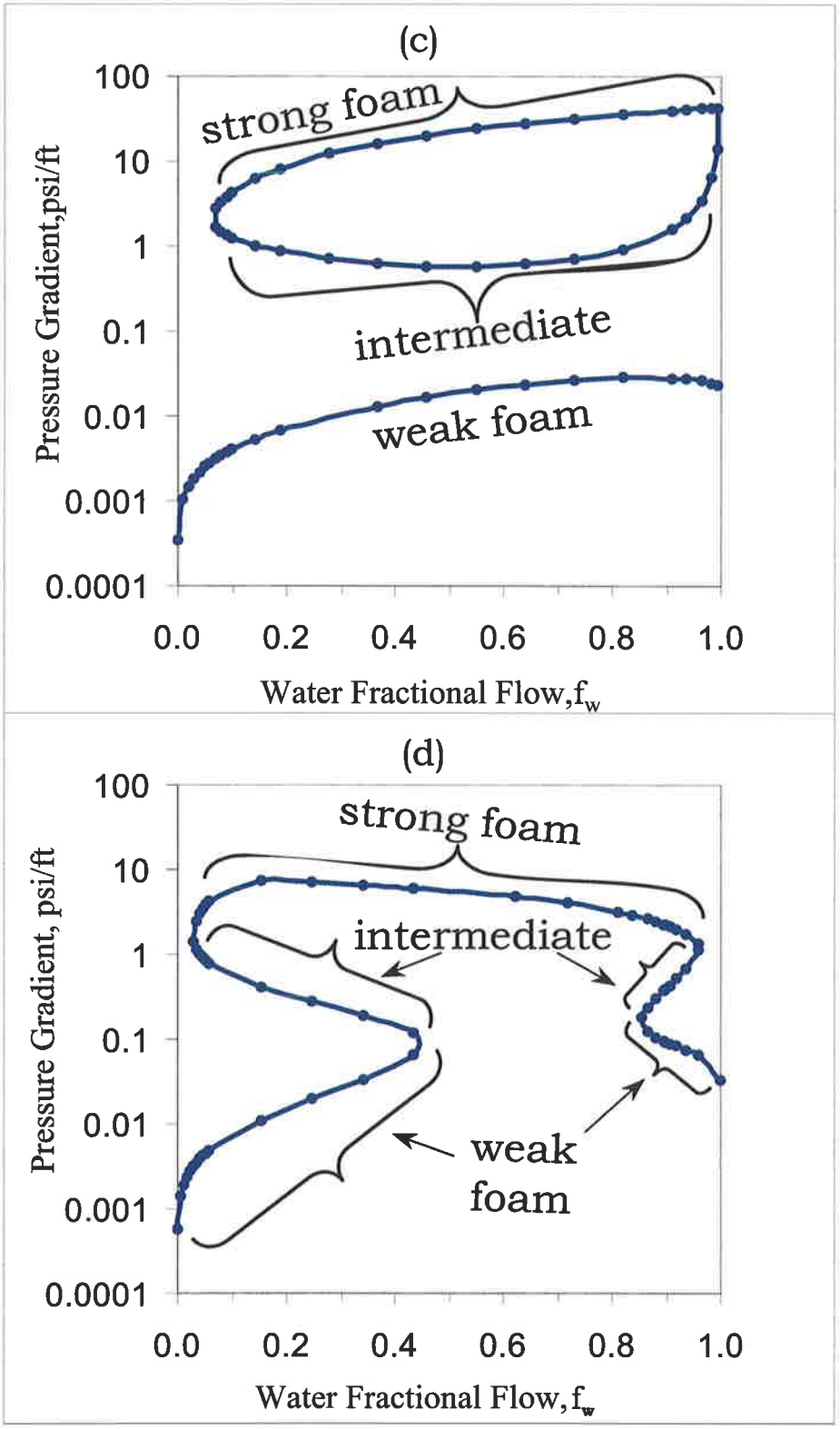

Fig. 4-16. Pressure gradient as a function of u_t (continued): (c) u_t = 2.91 ft/day (d) u_t = 4.91 ft/day.

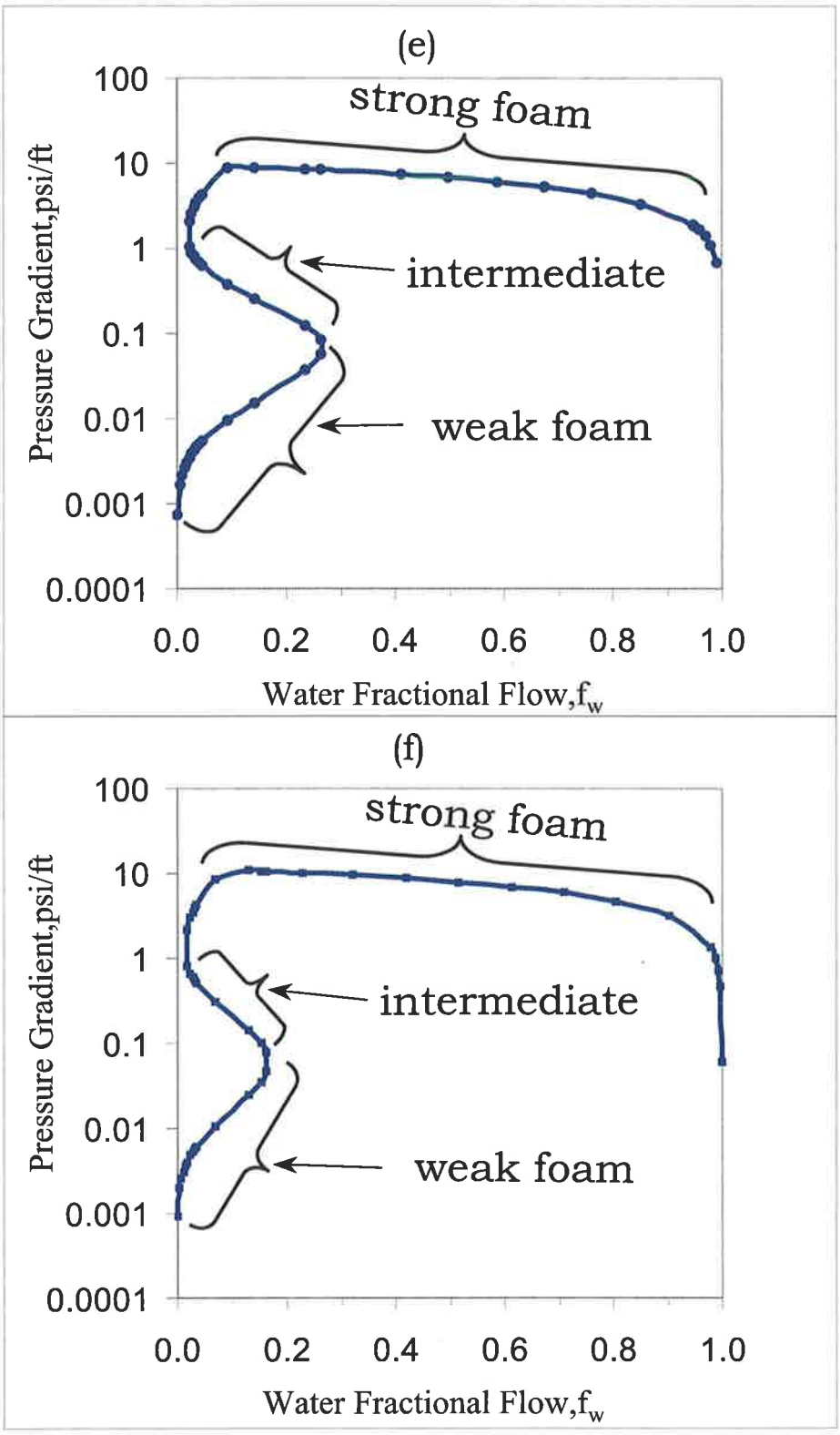

Fig. 4-16. Pressure gradient as a function of u_t (continued): (e) u_t = 6.37 ft/day (f) u_t =8.31 ft/day.

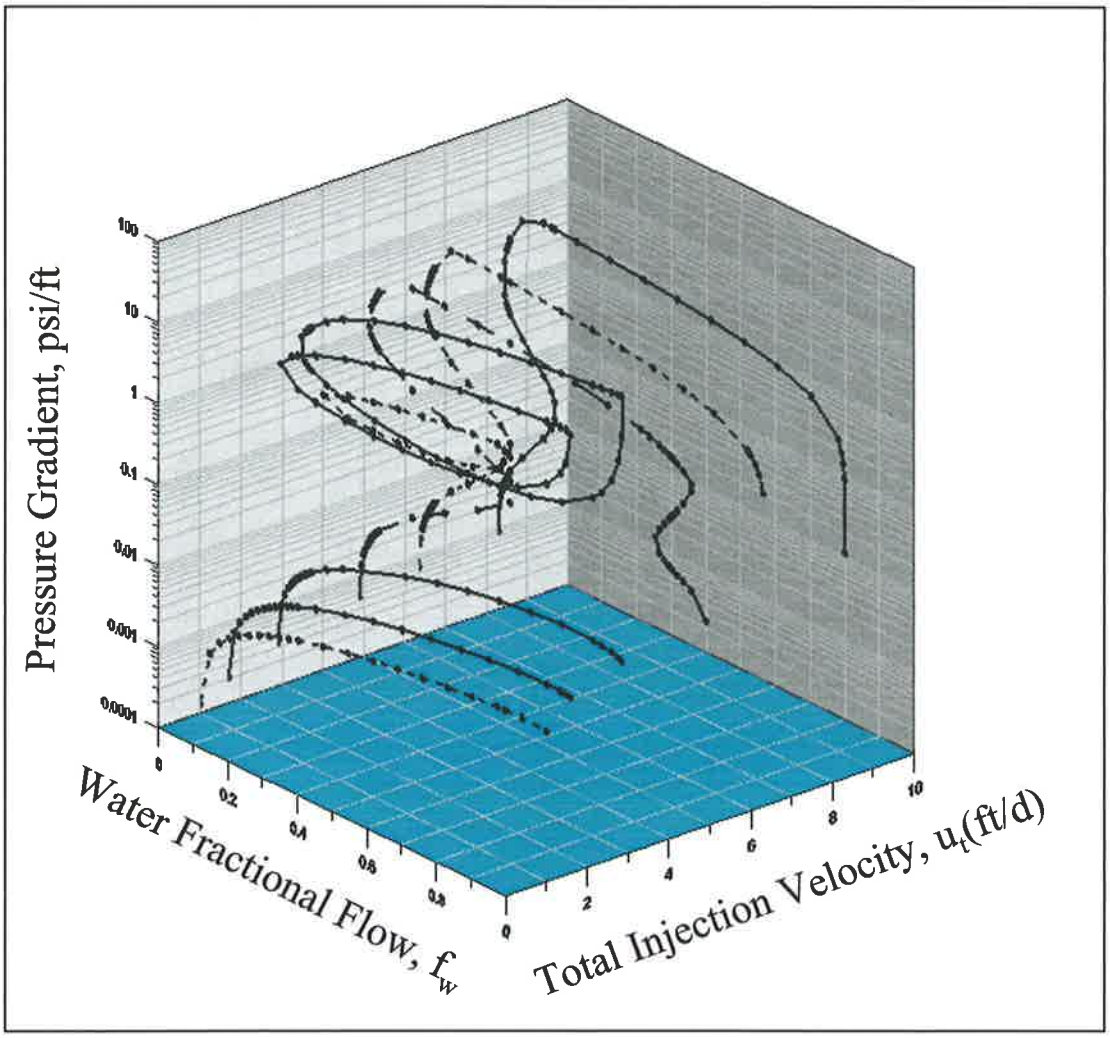

Fig. 4-17. Three dimensional representation of pressure gradient at different values of total injection rate (u_t).

One extreme case of foam application in porous media is gas injection into water-saturated porous media in which the injection condition is f_w=0. Previous studies [Kibodeaux and Rossen, 1997; Wassmuth *et al.*, 2001; Rossen and Bruining, 2004] show that the prediction of foam displacement during gas injection is very challenging because the mechanism seems to be hinged on the x-axis (*i.e.*, f_w=0).

Figs. 4-18 and 4-19 show examples of such cases at u_t = 5.89 ft/day. Note that this injection condition corresponds to (S_w, f_w) = (0.04, 0.0). In Fig. 4-18, the initial condition is followed by a shock and spreading waves, leading to weak-foam state that provides a moderate reduction in gas mobility and water saturation. Fig. 4-19 shows the formation of strong foam (with a significant reduction in gas mobility and water saturation near S_w^*) after the shock which is followed by the jump at the same S_w to reach the constant state of IJ. There are very slowly moving spreading waves between the injection condition (J) and the constant state (IJ).

It should be noted that the success of the entire foam application during gas injection relies on the condition after the shock. To make this point clear, the value of C_g/C_c is kept the same, but the dynamic parameter, C_c, is selected 0.1 and 10 in Figs. 4-20a and 4-20b respectively. The numbers in the figures represent the pore volume injected. At the time of breakthrough, the weak foam (*cf.*, Fig. 4-18) sweeps about 40% and, in contrast, the strong foam (*cf.*, Fig. 4-19) sweeps more than 92% of the porous media. Large value of C_c (also meaning large value of C_g if C_g/C_c is fixed) indicates active lamella creation and coalescence. Figs. 4-18 through 4-20 clearly show that among many possible solutions predicted by the fractional flow method, dynamics of foam rheology in porous media can be another parameter to determine actual displacement process.

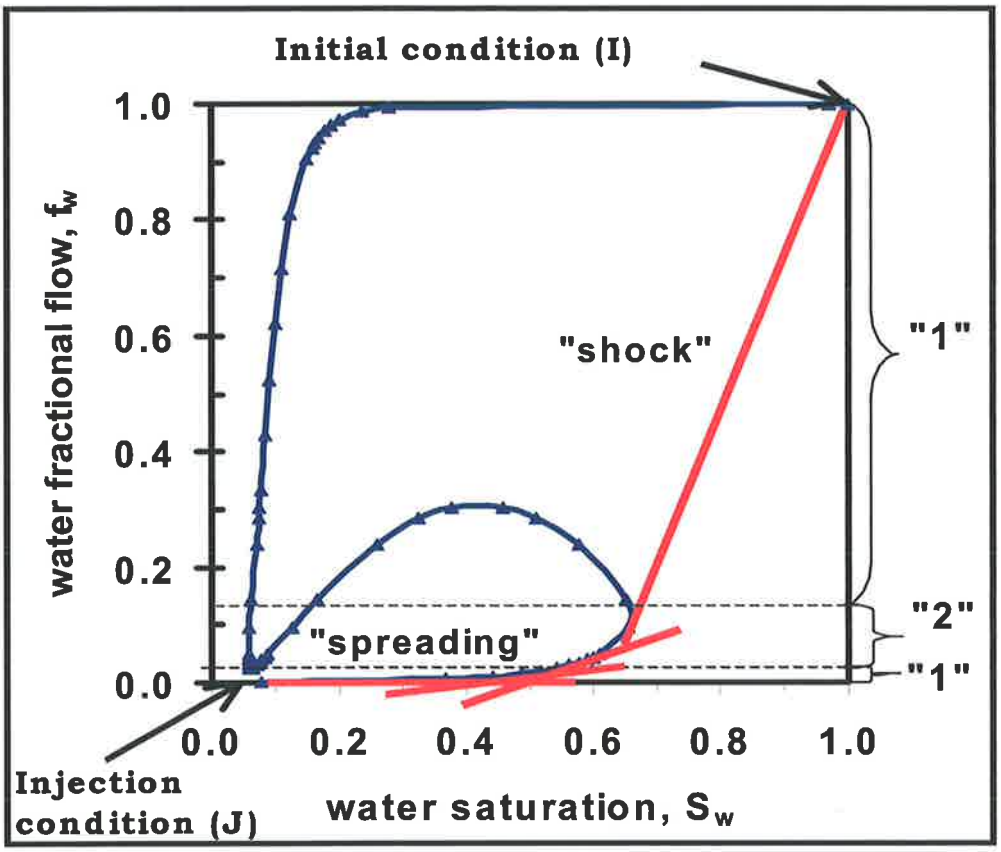

Fig. 4-18. Construction of fractional flow solution during gas injection (u_t = 5.89 ft/day) – weak foam propagation at C_c value of 0.1 (Numbers on the right-hand side show possible number of solutions at fixed-f_w injection conditions).

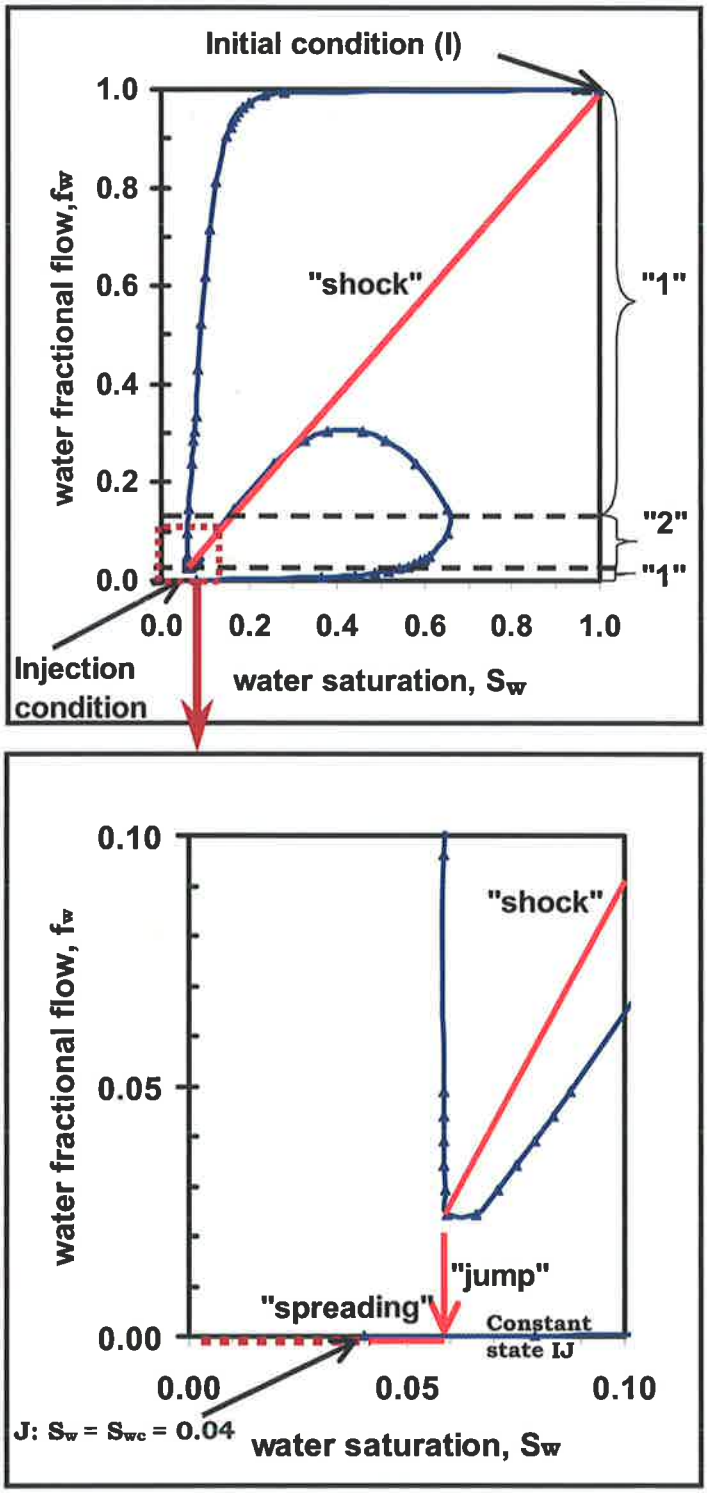

Fig. 4-19. Construction of fractional flow solution during gas injection (u_t = 5.89 ft/day) – strong foam propagation at C_c value of 10. (Numbers on the right-hand side show possible number of solutions at fixed-f_w injection conditions).

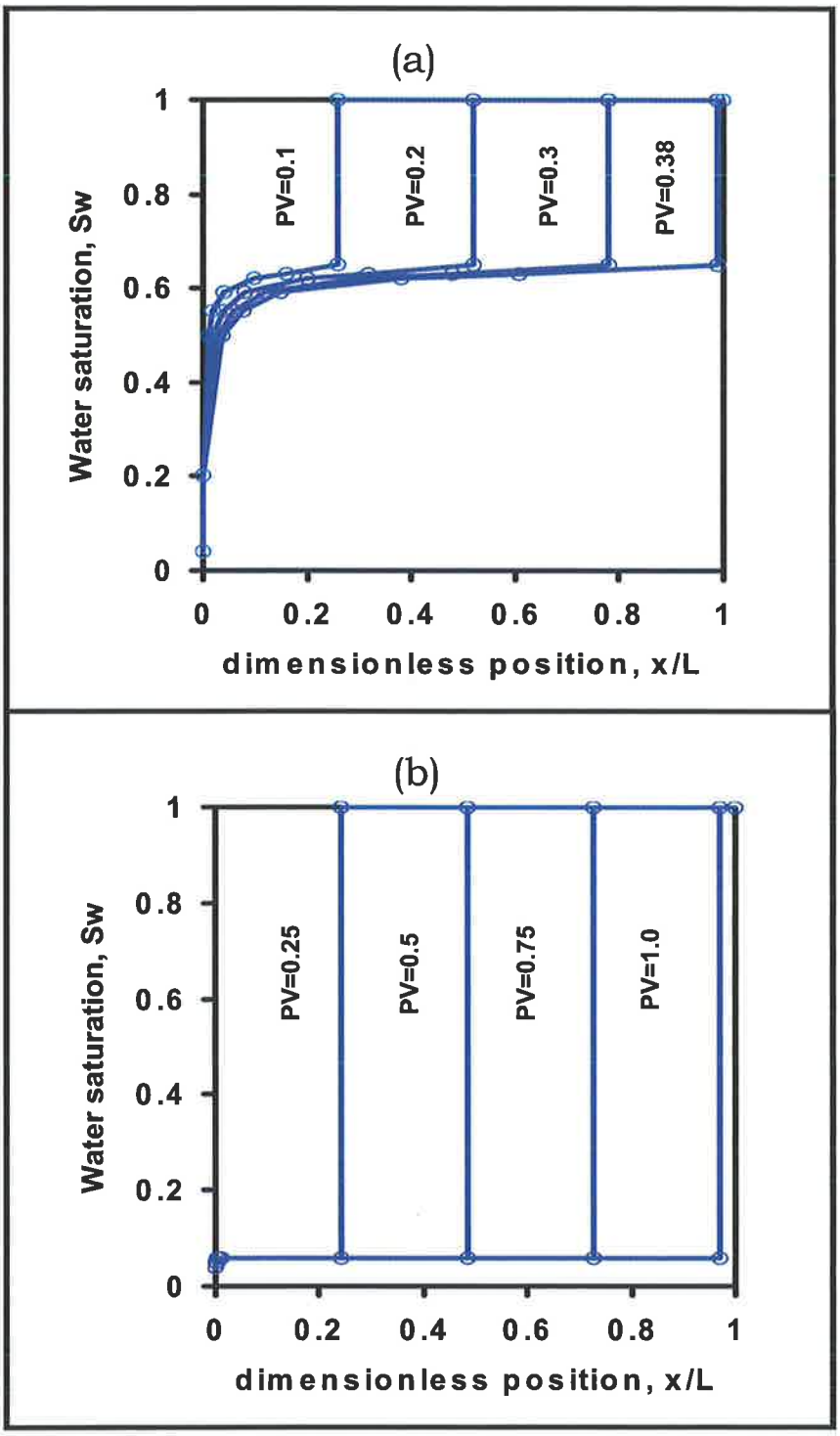

Fig. 4-20. Saturation profiles of the two different solutions to the cases shown in Figs. 4-18 and 4-19: (a) weak-foam propagation and (b) strong-foam propagation.

5. Conclusions and Future Work

5.1. Conclusions

Based on the findings explained in the earlier sections, one can summarize this study with the following conclusions:

1. Fractional flow curves were constructed incorporating mechanistic descriptions of foam rheology in porous media. The solution shows quantitatively how the shape of fractional flow curve changes with injection velocity: a weak-foam state is obtained at low injection velocity and a strong-foam is achieved at high injection velocity, which is in good agreement with the previous experimental studies. In between these two cases, there is a range of injection velocities in which the kinetics of lamella creation and coalescence governs the nature of foam propagation. Upon the construction of fractional flow curves, not all parts of the curves were valid and thus the solutions for physically invalid portions should be eliminated.

2. Fractional flow curves were analyzed in terms of water saturation, foam texture and pressure profile. The results were compared with simulation results for weak and strong foams. As expected, there was good consistency between analytical and numerical solutions, which proves the role of fractional flow theory to guide simulation studies. The peaks in foam texture at the leading edge of foam bank in the simulations, which do not appear in the fractional flow solutions, reflect complicated dynamics of foam physics in porous media. Because the fractional flow method assumes local steady state, this discrepancy, believed to be dependent upon grid-block and time-step sizes in numerical calculations, is not of importance in this study.

3. Mechanistic foam functions make it possible to keep track of the effect of injection velocities on foam propagation. Results are presented by a fractional flow surface in a three-dimensional space with total injection velocity in z-axis and water saturation and fractional flow in x- and y-axes respectively. The fractional flow curve at a specific value of injection velocity is no other than the slice of a three-dimensional surface parallel to the x-y plane. Constructing a three-dimensional fractional flow surface is believed

to be a convenient method to analyze velocity-dependent displacement process, as is the case with foam.

4. With the methodology developed in this study, it is possible to bring the foam fractional flow methods to more complicated situations such as gas injection, surfactant-alternating-gas (SAG) process, and foam displacement at very dry conditions in which the kinetics of abrupt lamella coalescence near the limiting capillary pressure plays a key role. The fractional flow theory is capable of providing mathematically reliable and robust solutions in these applications that often fail due to the instability and divergence near the singularity in the simulations.

5.2. Future work

The following aspects should be further investigated in line with this study:

1. The comparison between the simulation and fractional flow solutions in this study does not cover the case of strong foam in the high-quality regime. This is mainly due to the fact that foams in the high-quality regime are very sensitive to changes in P_c, and the drastic change in foam mobility within a very narrow range of S_w causes a singularity, resulting in instability and divergence of numerical simulation. This issue deserves further study. Building a mechanistic foam simulator that can handle foam behaviour near S_w^* should be a prerequisite.

2. The foam modelling and simulation technique introduced in this study should be extended to multi-dimensional space to guide field applications. Fractional flow theory can be used to predict steady-state foam behaviour in two-dimensional space which can serve as a basis for foam simulation in two- or three-dimensional space.

3. In many laboratory and field applications, gas phase is injected at fixed pressure while liquid phase is injected at fixed rate. As a result, the solutions to fractional flow curves at fixed-rate injection may not be relevant to the case of fixed-pressure injection because of the catastrophic nature of foam rheology in porous media. The continuity equation should be revisited to understand the implications of fixed-pressure boundary conditions.

4. The presence of oil can significantly distort some of the results observed in this study. Characterization of different types of oil and their effects on foam rheology in porous media is worth investigating. The effect of oil on foam mechanisms should be incorporated into mechanistic foam-simulation technique for field applications. The fractional flow theory is a useful tool to analyse displacement process, even in the presence of oil, as long as a local steady state is obtained instantaneously.

References

Alvarez, J.M., Rivas, H., and Rossen, W.R., 2001. A Unified Model for Steady-State Foam Behavior at High and Low Foam Qualities. *SPE J*, September 325-333.

Aronson, A.S., Bergeron, V., Fagan, M.E., and Radke, C.J., 1994. The Influence of Disjoining Pressure on Foam Stability and Flow in Porous Media. Colloids Surfaces A: *Physicochem. Eng. Aspects*, vol.83, 109.

Baghdikian, S.Y., and Handy, L.L., 1991. Transient Behaviour of Simultaneous Flow of Gas and Surfactant Solution in Consolidated Porous Media. Report, University of Southern California

Bernard, G.G., Holm, L.W., and Jacobs, W.L., 1965. Effect of Foam on Trapped Gas Saturation and on Permeability of Porous Media to Water. *SPE J*, December, 195-300.

Bertin, H.J., Quintard, M.Y., and Castanier, L.M., 1998. Development of a Bubble-Population Correlation for Foam-Flow Modeling in Porous Media. *SPE J*, December, 356-362.

Bikerman, J.J., 1973, Foams, Springer-Verlag, New York.

Blaker, T., Morten, G., Aarra, Skauge, A., Rasmussen, L., Harald K. Celius, Martinsen, H.A., Vassenden, F., 2002. Foam for Gas Mobility Control in the Snorre Field: The FAWAG Project. *SPEREE*, August, 317-323.

Buckley, S.E., and Leverett, M.C., 1941. Mechanism of Fluid Displacement in Sands. *Trans. AIME,* 146,107-116.

Chang, S.H., Owusu, L.A., French, S.B., 1990. The Effect of Microscopic Heterogeneity on CO2 -Foam Mobility: Part 2-Mechanistic Foam Simulation. SPE 20191, presented at the SPE/DOE Enhanced Oil Recovery Symposium, 22-25 April, Tulsa, Oklahoma.

Chang, S.H., and Grigg, R.B., 1996. Foam Displacement Modelling in CO2 Flooding Processes. SPE 35401, presented at the SPE/DOE Improved Oil Recovery Symposium, 21-24 April, Tulsa, Oklahoma.

Chambers, K.T., and Radke, C.J., 1991. Interfacial Phenomena in Petroleum Recovery. Morrow, M.R., (Ed), Marcel Dekker: New York, Chapter 6, 191-255.

Chen, M., Yortsos, Y.C., and Rossen, W.R., 2004. A Pore-Network Study of the Mechanisms of Foam Generation. SPE 90939, presented at the SPE Annual Technical Conference and Exhibition, 26-29 September, Houston, Texas.

Cheng, L., Kam, S.I., Delshad, M., and Rossen, W.R., 2002. Simulation of Dynamic Foam-Acid Diversion Processes. *SPE J,* September, 316-324.

Chou, S.I., 1990. Percolation Theory of Foam in Porous Media. SPE 20239, presented at the SPE/DOE Enhanced Oil Recovery Symposium, 22-25 April, Tulsa, Oklahoma.

Chou, S.I., 1991. Conditions for Generating Foam in Porous Media. SPE 22628, presented at the SPE Annual Technical Conference and Exhibition, 6-9 October, Dallas, Texas.

Collins, R.E., 1961. Flow of Fluids Through Porous Materials. Research & Engineering Consultants, Inc., Englewood, CO.

Dake, L.P., 1978. Fundamentals of Reservoir Engineering, Elsevier, New York.

Derjaguin, B.V., and Obukhov, E.V., 1936. *Acta Physicochim URSS*, 5(1), 1-22.

Fisher, A.W., Fousler, R.E., and Goodyear, S.G., 1990. Mathematical Modelling of Foam Flooding. SPE 20195, presented at the 1990 SPE/DOE Symposium on Improved Oil Recovery, Tulsa, OK.

Friedmann, F., and Jensen, J.A., 1986. Some Parameters Influencing the Formation and Propagation of Foams in Porous Media. SPE 15087, presented at SPE California Regional Meeting, 2-4 April, Oakland, California.

Friedmann, F., Chen, W.H., and Gauglitz, P.A., 1991. Experimental and Simulation Study of High-Temperature Foam Displacement in Porous Media. *SPERE*, February, 37-45.

Gauglitz, P.A., Friedmann, F., Kam, S.I., and Rossen, W.R., 2002. Foam Generation in Homogeneous Porous Media. *Chem. Eng. Sci.,* vol. 57, 4037-4052.

Hanssen, J.E., Holt, T., and Surguchev, L.M., 1994. Foam Processes: An Assessment of Their Potential in North Sea Reservoirs Based on a Critical Evaluation of Current Field Experience. SPE 27768, presented at the SPE/DOE Improved Oil Recovery Symposium, 17-20 April, Tulsa, Oklahoma.

Hirasaki, G.J., and Lawson, J.B., 1985. Mechanisms of Foam Flow Through Porous Media - Apparent Viscosity in Smooth Capillaries. *SPE J*, April 176-190.

Hirasaki, G.J., Miller, C.A., Szafranski, R., Lawson, J.B., and Akiya, N., 1997. Surfactant/Foam Process for Aquifer Remediation. SPE 37257, presented at the SPE International Symposium on Oilfield Chemistry, Houston, TX, February 18-21.

Hirasaki, G.J., 1989. The Steam-Foam Process. SPE 19518, *JPT*, May, 449-456.

Hirasaki, G.J., Jackson, R.E., Jin, M., Lawson, J.B., Londergan, J., Meinardus, H., Miller, C.A., Pope, G.A., Szafranski, R., and Tanzil, D., 2000. Field Demonstration of the Surfactant/Foam Process for Remediation of a Heterogeneous Aquifer Contaminated with DNAPL, in NAPL Removal: Surfactants, Foams, and Microemulsions. S. Fiorenza, C. A. Miller, C. L. Oubre, and C. H. Ward, (eds.), Lewis Publishers, Boca Raton.

Jiménez, A.I., and Radke, C.J., 1989. Oilfield Recovery: Enhanced Recovery and Production Stimulation. Borchardt, J.K., Yen, T.F., (Eds), ACS Symposium Series 396, *American Chemical Society*, Washington, DC, Chapter 25, 460-479.

Kam, S.I, Frenier, W.W, Davies, S.N, and Rossen, W.R, 2003. Experimental Study of High-Temperature Foam for Acid Diversion. SPE 82266, presented at the SPE European Formation Damage Conference, The Hague, The Netherlands, and 13-14 May.

Kam, S.I., and Rossen, W.R., 2003. A Model for Foam Generation in Homogeneous Porous Media. *SPE J*, vol. 8, December, 417-425.

Kam, S.I., Li, Q., Nguyen, Q.P., and Rossen, W.R., 2004. Dynamic Simulations With an Improved Model for Foam Generation. SPE 90938, presented at the SPE Annual Technical Conference and Exhibition, Houston, Texas, U.S.A., September 26-29.

Kharabaf, H., and Yortsos, Y.C., 1996. A Pore-Network Model For Foam Formation And Propagation in Porous Media. SPE 36663, *SPE J*, vol 3, No. 1, March, 42-53.

Khatib, Z.I., Hirasaki, G.J., and Falls, A.H., 1988. Effects of Capillary Pressure on Coalescence and Phase Mobilities in Foams Flowing Through Porous Media. *SPERE*, August, 919-926.

Khatib, Z.I., Hirasaki, G.J., and Falls, A.H., 1988. Effects of Capillary Pressure on Coalescence and Phase Mobilities in Foams Flowing Through Porous Media. *SPERE*, August , 919-926.

Kibodeaux, K.R, and Rossen, W.R, 1997. Coreflood Study of Surfactant-Alternating-Gas Foam Processes. SPE 38318, presented at the SPE Western Regional Meeting, Long Beach, CA, 25-27 June.

Kovscek, A.R., and Radke, C.J., 1994. Fundamentals of Foam Transport in Porous Media, in Foams: Fundamentals and Applications in the Petroleum Industry. L.L. Schramm (ed.), *ACS Advances in Chemistry Series* No. 242, Am. Chem. Soc., Washington, DC.

Kovscek, A.R., Patzek, T.W., and Radke, C.J., 1995. A Mechanistic Population Balance Model for Transient and Steady-State Foam Flow in Boise Sandstone. *Chem. Eng. Sci.*, vol. 50, 3783-3799.

Kovscek, A.R., Patzek, T.W., and Radke, C.J., 1997. Mechanistic Foam Flow Simulation in Heterogeneous and Multidimensional Porous Media. *SPE J*, December, 511-526.

Lake, L., 1989. Enhanced Oil Recovery. Prentice Hall, Englewood Cliffs, NJ.

Mahmood, S.M., Tariq, S.M., and Brigham, W.E., 1986. A Model for Prediction of Recovery and Pressure History for 2-D Displacement of Oil Through Porous Media by Gas/Surfactant. SPE 15076, presented at the SPE California Regional Meeting, 2-4 April, Oakland, California.

Mamun, C.K., Rong. J.G., Kam, S.I., Liljestrand, H.M., and Rossen, W.R., 2002. Extending Foam Technology from Improved Oil Recovery to Environmental Remediation. SPE 77557, presented at the SPE Annual Technical Conference, San Antonio, TX, 29 September-2 October.

Marfoe, C.H., and Kazemi, H., 1987. Numerical Simulation of Foam Flow in Porous Media. SPE 16709, presented at the SPE Annual Technical Conference and Exhibition, 27-30 September, Dallas, Texas.

Nguyen, Q.P., Alexandrov, A.V., Zitha, P.L., and Currie, P.K., 2002. Experimental and Modelling Studies on Foam in Porous Media: A Review. SPE 58799, presented at the SPE International Symposium on Formation Damage Control, 23-24 February, Lafayette, Louisiana.

Osterloh, W.T., and Jante, M.J., 1992. Effects of Gas and Liquid Velocity on Steady-State Foam Flow at High Temperature. SPE 24179, presented at the SPE/DOE Symposium on Enhanced Oil Recovery, Tulsa, OK, April 22-24.

Patzek, T.W., and Koinis, M.T., 1990. Kern River Steam-Foam Pilots. SPE 17380, *JPT*, April, vol. 42, 496-503.

Pope, G.A., 1980. The Application of Fractional Flow Theory to Enhanced Oil Recovery. *SPE J.*, No.10, 191-205.

Poston, T., and Stewart, I., 1978. Catastrophe Theory and Its Applications. Dover Publications, Inc., Mineola.

Ransohoff, T.C., and Radke, C.J., 1988. Mechanisms of Foam Generation in Glass-Bead Packs. *SPERE*, May, 573-585.

Rossen, W.R., and Gauglitz, P.A., 1990. Percolation Theory of Creation and Mobilization of Foam in Porous Media. *AIChE J*, vol. 36, 1176-1188.

Rossen, W.R., and Zhou, Z.H., 1995. Modelling Foam Mobility at the Limiting Capillary Pressure. *SPE Adv. Technol.*, vol. 3, 146.

Rossen, W.R., Kibodeaux, K.R., Shi, J.X., Zeilinger, S.C., and Lim, M.T., 1995. Injectivity and Gravity Override in Surfactant-Alternating-Gas Foam Processes. SPE 30753, presented at the SPE Annual Technical Conference and Exhibition, 22-25 October, Dallas, Texas.

Rossen, W.R., 1996. Foams in Enhanced Oil Recovery, in Foams: Theory, Measurements and Applications. R. K. Prud'homme and S. Khan (eds.). Marcel Dekker, New York.

Rossen, W.R., and Wang, M.W., 1999. Modelling Foams for Acid Diversion. *SPEJ*, June, 92-100.

Rossen, W.R., Zeilinger, S.C., Shi, J.X., and Lim, M.T., 1999. Simplified Mechanistic Simulation of Foam Processes in Porous Media. *SPE J*, vol. 4, 279-287, September.

Rossen, W.R., 2003. A Critical Review of Roof Snap-Off as a Mechanism of Steady-State Foam Generation in Homogeneous Porous Media. *Colloids Surfaces A: Physicochem Eng. Aspects*, vol. 225 , 1-24.

Rossen, W.R., and Bruining, J., 2004. Foam Displacements With Multiple Steady States. Presented at the SPE/DOE Symposium on Improved Oil Recovery, Tulsa, OK, 17–21 April.

Sanchez, J.M., and Schechter, R.S., 1989. Surfactant Effects on the Two-Phase Flow of Steam-Water and Nitrogen-Water Through Permeable Media. *J.Petr.Sci.Eng.*, vol. 3, 185-199.

Schramm, L.L. (ed.), 1994. Foams: Fundamentals and Applications in the Petroleum Industry. *ACS Advances in Chemistry Series* No. 242, Am. Chem. Soc., Washington, DC.

Shan, D., and Rossen, W.R., 2002. Optimal Injection Strategies for Foam IOR. SPE 75180, presented at the SPE/DOE Improved Oil Recovery Symposium, 13-17 April, Tulsa, Oklahoma.

Tanzil, D., 2001. Foam Generation and Propagation in Heterogeneous Porous Media. PhD thesis, Rice University, March.

Tanzil, D., Hirasaki, G.J., and Miller, C.A., 2002. Conditions for Foam Generation in Homogeneous Porous Media. SPE 75176, presented at the SPE/DOE Symposium on Improved Oil Recovery, Tulsa, OK, 13-17 April.

Wang, D., Cheng, J., Yang, Z., Li, Q., Wu, W., and Yu, H., 2001. Successful Field Test of the First Ultra-Low Interfacial Tension Foam Flood. SPE 72147, presented at SPE Asia Pacific Improved Oil Recovery Conference, 6-9 October, Kuala Lumpur, Malaysia.

Wassmuth, F.R., Green, K.A., and Randall, L., 2001. Details of In-Situ Foam Propagation Exposed With Magnetic Resonance Imaging. *SPEREE*, April, 135-149.

Wassmuth, F.R., Green, K., and Hodgins, L., 2004. Water Shutoff in Gas Wells: Proper Gel Placement Is the Key to Success. SPE 89403, presented at SPE/DOE Symposium on Improved Oil Recovery, 17-21 April, Tulsa, Oklahoma.

Zeilinger, S.C., 1996. A Modelling and Experimental Study of Foam in Acid Diversion and Enhanced Oil Recovery, Ph.D dissertation, The University of Texas at Austin.

Appendix A: Algorithm for constructing fractional flow curves

1. Specify total superficial velocity (u_t). Starting with the lowest possible number, a value for water superficial velocity (u_w) is selected. Note that $u_g = u_t - u_w$.

2. Assume values for water saturation (S_w) between 0 and 1.

3. Determine water relative permeability (k_{rw}) from

$$k_{rw} = 0.7888\left(\frac{S_w - S_{wc}}{1 - S_{wc} - S_{gr}}\right)^{1.9575}.$$

4. Determine pressure gradient (∇p) from $\nabla p = \frac{u_w \mu_w}{k k_{rw}}$.

5. Calculate foam texture (n_f) from $n_f = \left(\frac{C_g}{C_c}\right)(S_w - S_w^*)^n S_w (\nabla p)^m$.

6. Determine gas relative permeability in absence of foam (k_{rg}^0) from

$$k_{rg}^{\ 0} = \left(\frac{1 - S_w - S_{gr}}{1 - S_{wc} - S_{gr}}\right)^{2.2868}.$$

7. Calculate gas velocity in absence of foam (u_g^0) from $u_g^{\ 0} = \frac{k k_{rg}^{\ 0} \nabla p}{\mu_g}$.

8. Assume a value for u_g and calculate a new u_g from

$$u_{g\,calculated} = \frac{k k_{rg}^{\ 0} \nabla p}{\mu_g^{\ 0} + \left(C_f n_f / u_{g\,assumed}\right)^{1/3}}.$$

This calculation can be repeated until $u_{g\ calculated}$ and $u_{g\ assumed}$ values converge. This value is recorded as gas velocity in presence of foam (u_g^f). The calculation for u_g^f uses a subroutine within the Excel spreadsheet which has been explained in Appendix B

9. Calculate water fractional flow (f_w) from $f_w = \frac{u_w}{u_w + u_g^f}$.

10. Select the sets of (S_w, f_w) giving u_g^f in step 8 equal to u_g in step 1.

11. Increase the value of u_w in step 1 and repeat steps 1 through 10 to obtain another set of (S_w, f_w) values.

12. Continue step 11 for a wide range of u_w's (*i.e.*, $0 \leq u_w \leq u_t$).

13. Plot the fractional flow curve using calculated outcomes.

A.1. Steps for generating the saturation profile

A saturation profile is a plot of dimensionless distance (on x-axis) against water saturation (on y-axis). Such a plot allows one to track the movement of the floodfront from the injector to the producer. The following steps describe the manner in which the saturation profiles were generated:

1. Draw a straight line from the initial condition "I" to the fractional flow curve. In this study, the initial condition in all cases is a core 100% saturated with surfactant solution.

2. Identify the point of tangency of the straight line to the curve. This is the position of the shockfront or the leading edge of the front. S_{wf} and f_{wf} give the corresponding saturation and water fractional flows at this point respectively. Calculate graphically the slope of the tangent as df_{wf}/dS_{wf}. This gives the dimensionless velocity of the wave at the shockfront.

3. The part of the curve between (S_{wf}, f_{wf}) and the injection condition "J" is the spreading wave. Choose a number of saturation points between (S_{wf}, f_{wf}) and "J" and draw tangents to each of these selected saturation points. The slopes of these tangents give the velocities of the waves at each of these saturations.

4. Similarly, calculate the velocity of the wave at the injection point.

5. Calculate dimensionless distance (x_D) from the equation

$$x_D = t_D \times v \qquad \text{(A-1)}$$

where t_D is the time in pore volumes injected and v is the velocity at different saturations as calculated in steps 2, 3 and 4.

6. Plot the calculated x_D values on x-axis and the corresponding water saturations on y-axis to obtain the saturation profile.

A.2. Steps for generating the foam texture profile

1. Read the values of n_f from the Excel spreadsheet corresponding to S_w value at the shockfront, at the points chosen along the spreading wave, and at the injection point.

2. Plot the x_D values calculated from the saturation profile on the x-axis against the corresponding n_f values on the y-axis to obtain the foam texture profile.

A.3. Steps for generating the pressure profile

1. Read the ∇p values from the Excel spreadsheet corresponding to the chosen S_w values.

2.Calculate the pressure at each saturation using the following finite difference equation

$$p_i = p_{i-1} + \left[\Delta x \nabla p_i\right] \qquad \text{, I = 1 to N} \qquad \text{(A-2)}$$

where Δx is the grid block size in x-axis and N is the total number of grids along x-direction.

3. Plot the x_D values calculated from the saturation profile on the x-axis against the corresponding pressure values on the y-axis to obtain the pressure profile.

Appendix B: Sub-routine for calculating gas velocity in presence of foam

```
Function Ugfoam (ugo, K, Krgo, Dp, mugo, Cf, nf)

ugold = ugo
ugnew = ugo / 2
n = 0
deviation = 0.0001

Do Until Abs((ugold - ugnew) / ugnew) < deviation

   ugnew = (K * Krgo * Dp) / (mugo + ((Cf * nf) * (ugold ^ (-1 / 3))))

   If
     Abs((ugold - ugnew) / ugnew) < deviation Then
      GoTo 10

   Else
      ugold = (ugnew + 2 * ugold) / 3

   End If
   n = n + 1
   If (n > 500) Then
      Ugfoam = n
      GoTo 20
   End If

Loop

10 Ugfoam = ugnew

20 End Function
```